

CALIFORNIA INSTITUTE OF TECHNOLOGY

EARTHQUAKE ENGINEERING RESEARCH LABORATORY

**THE FOURIER TRANSFORM, RESPONSE
SPECTRA AND THEIR RELATIONSHIP
THROUGH THE STATISTICS OF
OSCILLATOR RESPONSE**

BY

F. E. UDWADIA AND M. D. TRIFUNAC

REPORT NO. EERL 73-01

A REPORT ON RESEARCH CONDUCTED UNDER GRANTS FROM THE NATIONAL
SCIENCE FOUNDATION AND THE EARTHQUAKE RESEARCH AFFILIATES
PROGRAM AT THE CALIFORNIA INSTITUTE OF TECHNOLOGY

PASADENA, CALIFORNIA

APRIL 1973

CALIFORNIA INSTITUTE OF TECHNOLOGY
EARTHQUAKE ENGINEERING RESEARCH LABORATORY

THE FOURIER TRANSFORM, RESPONSE SPECTRA
AND THEIR RELATIONSHIP THROUGH THE
STATISTICS OF OSCILLATOR RESPONSE

by

F. E. Udwadia and M. D. Trifunac

Report No. EERL 73-01

A report on research conducted under grants from the National
Science Foundation and the Earthquake Research Affiliates
Program at the California Institute of Technology

Pasadena, California

April 1973

ABSTRACT

The concept of the Damped Fourier Transform (D. F. S.) has been developed through an understanding of the nature of the response of a damped oscillator to input ground accelerations. It has been shown that such a transform serves as a lower bound to the corresponding damped velocity spectrum curves.

A review of the statistics of the maxima of a random function has been done and its application to the determination of response spectrum estimates has been studied. Such simple statistical estimates have been found to be very useful in improving our physical understanding of response spectra.

INTRODUCTION

In Earthquake Engineering and Strong Motion Seismology, Fourier techniques present an important tool in understanding and interpreting the frequency content of various time signals. Ambient vibration tests⁽¹⁾, source mechanism studies⁽²⁾, response spectrum analyses⁽³⁾ and instrument correction techniques⁽⁴⁾ are only some of the examples in which Fourier representations are widely used.

This paper attempts to study some of the specific properties of these transform methods in the context of vibration theory. Starting with the undamped oscillator, the concept of the Fourier transform is extended to damped oscillations defining the damped Fourier transforms. A comparison of these damped transforms and damped velocity spectrum curves is done. Smoothing techniques in the light of these results are discussed.

The second part of this work deals with the applications of some well known results from the theory of random functions. The purpose of that section is to present the physical relations that exist between the Fourier transforms and the response spectra as seen from the probability point of view. It is shown that the computation of the response spectra based on the statistics of maxima of stationary functions is simple and economical, but it represents only the first approximation when compared with the actual response to real earthquakes. Comparisons of the damped Fourier spectrum, computed velocity spectra, and statistically calculated maximum responses are presented for random stationary processes and real earthquakes.

I. ANALYSIS OF FOURIER AMPLITUDE AND PHASE SPECTRA

The Undamped Oscillator

Some of the basic results from the theory of undamped oscillations will be reviewed here, so that extensions can then be easily made.

The governing equation for the relative response, $x(t)$, of an undamped oscillator subjected to an absolute base acceleration, $\ddot{a}(t)$, is given by

$$\ddot{x} + \omega_n^2 x = -\ddot{a}(t) \quad (1)$$

where ω_n (Fig. I. 1a) is the natural frequency of the oscillator. Equation (1) can be transformed into a first order equation through the substitution

$$\eta(\omega_n, t) = \dot{x}(t) + i\omega_n x(t)$$

to give

$$\frac{d\eta}{dt} - i\omega_n \eta = \ddot{z}(t), \quad (2)$$

where

$$\ddot{z}(t) = -\ddot{a}(t).$$

The solution $\eta(\omega_n, t)$ of Equation (2) which shall be henceforth referred to as the complex response of the oscillator, is given by

$$\eta(\omega_n, t) = \exp(i\omega_n t) \left[\int_0^t \ddot{z}(\tau) \exp(-i\omega_n \tau) d\tau + \eta_0 \right]. \quad (3)$$

Here η_0 is the value of η at $t=0$. The real and imaginary parts of this complex response can be further studied as follows.

Consider a new function $\ddot{z}^*(t)$ such that

$$\ddot{z}^*(t) = \begin{cases} \ddot{z}(t) & 0 \leq t \leq t_0 \\ 0 & \text{elsewhere.} \end{cases} \quad (4)$$

Then Equation (3) can be expressed as

$$\begin{aligned}\eta(\omega_n, t_0) &= \dot{x}(t_0) + i\omega_n x(t_0) \\ &= \exp(i\omega_n t_0) \int_{-\infty}^{\infty} \ddot{z}^*(\tau) \exp(-i\omega_n \tau) d\tau + \eta_0 \exp(i\omega_n t_0) \quad (5)\end{aligned}$$

In particular, at the natural frequencies

$$\omega_n^m = \frac{2\pi m}{t_0}, \quad m = 1, 2, \dots,$$

Equation (5) reduces to

$$\begin{aligned}\eta(\omega_n^m, t_0) &= \dot{x}(\omega_n^m, t_0) + i\omega_n^m x(\omega_n^m, t_0) \\ &= \int_{-\infty}^{\infty} \ddot{z}^*(\tau) \exp(-i\omega_n^m \tau) d\tau + \eta_0 \\ &= \left[X(\omega_n^m, t_0) + \dot{x}_0 \right] + i \left[Y(\omega_n^m, t_0) + \omega_n^m x_0 \right] \quad (6)\end{aligned}$$

where $X(\omega_n^m, t_0)$ and $Y(\omega_n^m, t_0)$ are the real and imaginary parts of the Fourier transform of $\ddot{z}^*(t)$ evaluated at the frequency $\omega_n^m = 2\pi m/t_0$, and, x_0 and \dot{x}_0 are the initial displacement and velocity respectively of an undamped oscillator of natural frequency ω_n^m .

Relation (6) can be interpreted as follows: The velocity at time $t=t_0$ of an undamped oscillator starting from rest ($x_0 = \dot{x}_0 = 0$) at $t=0$ and having a natural frequency $\omega_n^m = 2\pi m/t_0$ is given by the real part of the Fourier transform of the function $\ddot{z}^*(t)$ (defined in Equation (4)) calculated at the frequency ω_n^m . Similar interpretations can be made regarding the relation between the imaginary part of the transform and the pseudo-velocity of the oscillator at time $t=t_0$. On the other hand, by setting $\ddot{z}(t) \equiv 0$, for all t in Equation (6), we get the free vibration problem. If the time t_0 of observation is a complete multiple of the fundamental period of the oscillator, then the velocity and displacement of the oscillator at

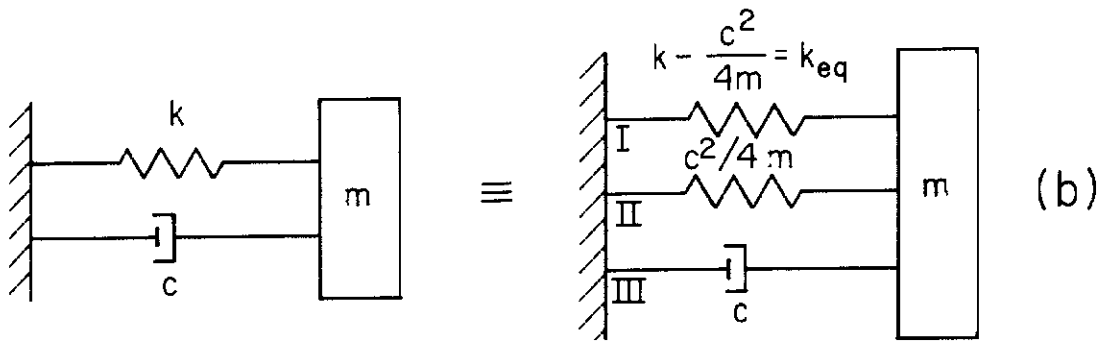
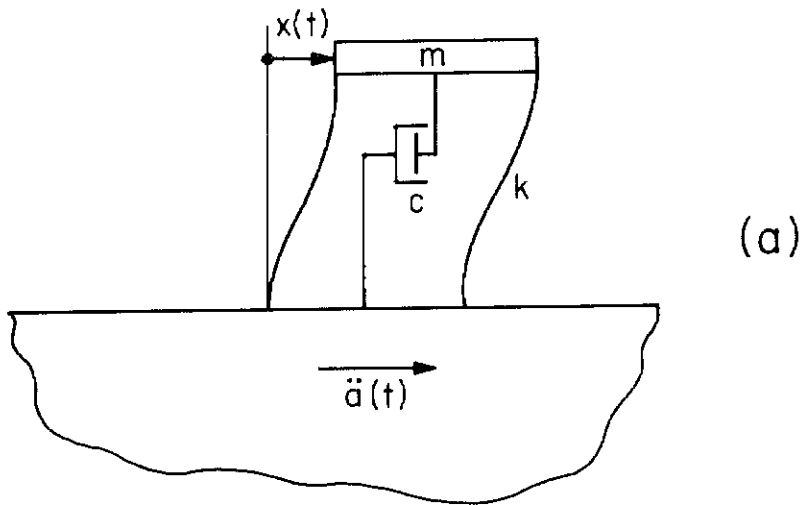


Figure I. 1 (a) A single degree of freedom oscillator subjected to ground acceleration $\ddot{a}(t)$.
(b) A mass-spring-dashpot system and its equivalent as interpreted through the phase of the complex variable η_d .

time t_0 will be identical to the initial velocity and displacement. Simplifying Equation (6) we have

$$\dot{x}(\omega_n^m, t_0) = X(\omega_n^m, t_0) + \dot{x}_0$$

and

$$x(\omega_n^m, t_0) = \left(\frac{2\pi m}{t_0}\right)^{-1} Y(\omega_n^m, t_0) + x_0.$$

Thus the presence of a set of initial conditions on an oscillator of natural frequency ω_n^m causes the velocity and displacement of such an oscillator at time t_0 to be shifted by constants equal to the initial velocity and displacement. We note that since the real and imaginary parts of the transform of $\dot{z}^*(t)$ are related to the velocity and the displacement of an oscillator (Equation (7)), they are not independent of each other. This would constitute a physical proof for the theorem of causality⁽⁵⁾ which states that for a real causal function the real and imaginary components of its transform must be related to each other.

The complex response $\eta(\omega_n, t_0)$ can also be expressed in terms of its phase and amplitude as

$$\eta(\omega_n, t_0) = \sqrt{e} \exp(i\varphi_n),$$

where, φ is the phase of the complex response and \sqrt{e} is its amplitude. We shall now show that the phase φ_n is related to the partition of the oscillator energy, and that for the specific oscillator frequencies $\omega_n = \omega_n^m$ it is identical to the corresponding phase of the Fourier transform. We have,

$$\tan^2 \varphi_n(t) = \left(\frac{\omega_n x(t)}{\dot{x}(t)}\right)^2 = \left(\frac{\text{Pseudo Velocity}}{\text{Velocity}}\right)^2 = \left(\frac{\text{Potential Energy at time } t}{\text{Kinetic Energy at time } t}\right).$$

For $\omega_n = \omega_n^m$ and $x_0 = \dot{x}_0 = 0$

$$\tan \varphi_n^m(t_0) = \frac{Y(\omega_n^m, t_0)}{X(\omega_n^m, t_0)} = \tan \psi(\omega_n^m, t_0) \quad (9)$$

where ψ is the phase of the transform of $\ddot{z}^*(t)$. The numerator in Equation (8) is the Potential Energy in the spring element while the denominator is the Total Energy less the Potential Energy in the system. The formulation of Equation (8) in this manner will be useful later on in the understanding of damped oscillators whose phase relations will be shown to be similar to those expressed above. The phase ψ of the transform then gives information on the partition of energy at time t_0 in an undamped oscillator of frequency ω_n^m with zero initial conditions ($\eta_0 = 0$). For durations of time, t_0 , which are not complete multiples of the oscillator period, the partition of energy would not be definable in such a simple manner.

Further insight into Equation (8) is obtained first through the substitution $t_0 - t = t_1$ in Equation (5) and then through a splitting of the function $\ddot{z}^*(t_0 - t_1)$ into its even and odd parts.

For $\eta_0 = 0$

$$\begin{aligned} \dot{x}(t_0) + i\omega_n x(t_0) &= \int_{-\infty}^{\infty} [\varphi(t_1) + \psi(t_1)] e^{i\omega t_1} dt_1 \\ &= \int_{-\infty}^{\infty} \varphi(t_1) \cos \omega t_1 dt_1 + i \int_{-\infty}^{\infty} \psi(t_1) \sin \omega t_1 dt_1 \end{aligned}$$

where $\varphi(t_1)$ and $\psi(t_1)$ are the even and odd parts of $\ddot{z}^*(t_0 - t_1)$ respectively. The velocity of the oscillator is then related to the even part of the function and the displacement to the odd part. Also,

$$\tan \varphi_n(t_0) = \frac{\int_{-\infty}^{\infty} \psi(t_1) \sin \omega t_1 dt_1}{\int_{-\infty}^{\infty} \varphi(t_1) \cos \omega t_1 dt_1} . \quad (10)$$

Assuming now that at $\omega = \omega^*$, $\tan \varphi = 0$, we have

$$\int_{-\infty}^{\infty} \psi(t_1) \sin \omega^* t_1 dt_1 = 0.$$

Letting $\omega = \omega^* + \Delta\omega$, the numerator of Equation (10) becomes

$$\begin{aligned} & \int_{-\infty}^{\infty} \psi(t_1) \sin(\omega^* + \Delta\omega) t_1 dt_1 \\ & \approx \int_{-\infty}^{\infty} \psi(t_1) \sin \omega^* t_1 \left[1 - \frac{(\Delta\omega t_1)^2}{2} + \dots \right] dt_1 \\ & + \int_{-\infty}^{\infty} \psi(t_1) \cos \omega^* t_1 \left[\Delta\omega t_1 + \dots \right] dt_1 \quad \text{for } |\Delta\omega t_0| \ll 1. \end{aligned}$$

If the phase $\varphi = 0$ at $\omega = \omega^* + \Delta\omega$,

$$\int_{-\infty}^{\infty} \psi(t_1) \sin \omega^* t_1 \frac{(\Delta\omega t_1)^2}{2} dt_1 = \int_{-\infty}^{\infty} \psi(t_1) \cos \omega^* t_1 \Delta\omega t_1 dt_1.$$

Thus for small $\Delta\omega$, $\tan \varphi$ will be zero if

$$\Delta\omega = \frac{2 \int_{-\infty}^{\infty} t_1 \psi(t_1) \cos \omega^* t_1 dt_1}{\int_{-\infty}^{\infty} t_1^2 \psi(t_1) \sin \omega^* t_1 dt_1} . \quad (11)$$

It may be noted that except in the case of no oscillation both numerator and denominator in Equation (10) cannot go to zero together, since they are proportional to the Potential and Kinetic energies respectively. Hence, the spacing between the consecutive zeroes in the phase angle will be decreased

as the duration of the record increases and as the function $\psi(t_1)$ (and hence $z^*(t_0 - t_1)$) has larger and larger contributions at longer and longer times.

The energy of the oscillator, E , at any time t is defined as

$\frac{1}{2}m(\dot{x}^2 + \omega_n^2 x^2) = \frac{1}{2}m|\eta|^2$. Hence for an oscillator with zero initial conditions

$$|\eta|^2 = \frac{2E}{m} = \left| \int_{-\infty}^{\infty} \ddot{z}^*(t) \exp(-i\omega_n t) dt \right|^2 \equiv e \quad (12)$$

where e equals twice the energy per unit mass. The energy of such an oscillator is not conserved since the system gains energy from the source of the external field.

As mentioned earlier the complex variable η can be looked upon as a vector in the phase plane (x, \dot{x}) . From Equation (12) the magnitude of this vector equals \sqrt{e} while its phase angle is given by Equation (8). The rate at which this vector rotates about the origin can be obtained as follows:

$$\tan \varphi_n = \frac{\omega_n x}{\dot{x}}$$

Using Equation (1),

$$\frac{d\varphi_n}{dt} = \omega_n \left[\frac{\dot{x}^2 + \omega_n^2 x^2 + x\ddot{a}}{\dot{x}^2} \right] \cos^2 \varphi_n = \omega_n \left[1 + \frac{x\ddot{a}}{e} \right] \quad (13)$$

Relation (13) indicates that for the free vibration problem the energy vector \vec{e} rotates at the natural frequency ω_n about the origin. For forced vibrations, the rate of rotation at any time will depend on the value of $\ddot{a}(t)$ and the value of $e(t)$ at that particular time.

The relative velocity response spectrum $S_V(\omega_n)$ value at frequency ω_n can be defined as $|\eta|_{\max}$ for when \dot{x} is a maximum, $x=0$ so that

$|\eta|_{\max} = |\dot{x}|_{\max}$. The modulus of the Fourier Transform gives the value $|\eta|_{t=t_0}$, and hence serves as a lower bound to the velocity spectrum value defined as $|\eta|_{\max}$.

The Damped Fourier Spectrum

The results of the previous section will now be extended to define the Damped Fourier Spectrum (D. F. S.) which will bear the same relation to the damped oscillator response as the Fourier spectrum bore to the undamped oscillator response.

The governing equation of relative response $x(t)$ of a damped linear oscillator subjected to an absolute base acceleration $\ddot{a}(t)$ is

$$\ddot{x} + 2\omega_n \xi \dot{x} + \omega_n^2 x = -\ddot{a} \equiv \ddot{z}(t) \quad (14)$$

where ξ is the percentage of critical damping.

Using the transformation $y = xe^{\alpha t}$ with $\alpha = \omega_n \xi$ we have

$$\ddot{y} + \omega_n^2 (1 - \xi^2) y = \ddot{z}(t) e^{\omega_n \xi t}$$

or

$$\ddot{y} + \omega_d^2 y = \ddot{z}(t) e^{\omega_d \beta t} \quad (14')$$

where $\omega_d = \omega_n \sqrt{1 - \xi^2}$, the damped natural period of the oscillator, and $\beta = \xi / \sqrt{1 - \xi^2}$.

The damping thus has led to an exponential increase in the forcing function of the reduced undamped system as seen from Equation (14'). As before, we define the complex variable $\eta_d^* = \dot{y} + i\omega_d y$. The solution of Equation (14) is as before

$$\eta_d^*(t_0) = \exp(i\omega_d t_0) \left\{ \int_0^{t_0} \ddot{z}(t) e^{\omega_d \beta t - i\omega_d t} dt + \eta_{d_0}^* \right\} \quad (15)$$

and $\eta_{d_0}^*$ is the value of η_d^* at time $t=0$. Application of Equation (15) to the time history $\ddot{z}(t)$ would lead to the determination of the damped oscillator response. However, better understanding of the problem is achieved if

we infer the nature of the damped system response directly from the response of an undamped oscillator. To do this we take the integrand in Equation (15) as a product of two functions $g(t)$ and $\ddot{z}^*(t)$, where

$$g(t) = \begin{cases} e^{(\omega_n \xi - i\omega_n \sqrt{1-\xi^2})t} & -\infty < t < t_0 \\ 0 & \text{otherwise} \end{cases} \quad (16a)$$

for $\xi > 0$ and $\omega_n > 0$ and

$$\ddot{z}^*(t) = \begin{cases} \ddot{z}(t) & 0 \leq t \leq t_0 \\ 0 & \text{otherwise} \end{cases} \quad (16b)$$

First we recall Parseval's formula,

$$I \equiv \int_{-\infty}^{\infty} \ddot{z}^*(t)g(t) dt = \frac{1}{2\pi} \int_{-\infty}^{\infty} Z(-\lambda)G(\lambda) d\lambda$$

where

$$Z(\lambda) = \int_{-\infty}^{\infty} \ddot{z}^*(t)e^{-i\lambda t} dt$$

and

$$G(\lambda) = \int_{-\infty}^{\infty} g(t)e^{-i\lambda t} dt.$$

Using the definition of $g(t)$ from Equation (16)

$$G(\lambda) = \int_{-\infty}^{t_0} e^{(\omega_n \xi - i\omega_n \sqrt{1-\xi^2})t} e^{-i\lambda t} dt,$$

there follows

$$G(\lambda) = \frac{e^{[\omega_n \xi - i(\omega_n \sqrt{1-\xi^2} + \lambda)]t_0}}{\omega_n \xi - i(\omega_n \sqrt{1-\xi^2} + \lambda)}. \quad (17)$$

Hence,

$$\begin{aligned}
 I &= \frac{1}{2\pi} \int_{-\infty}^{\infty} Z(-\lambda) \frac{e^{[\omega_n \xi - i(\omega_n \sqrt{1-\xi^2} + \lambda)]t_0}}{\omega_n \xi - i(\omega_n \sqrt{1-\xi^2} + \lambda)} d\lambda \\
 &= \frac{1}{2\pi} \int_{-\infty}^{\infty} Z(\lambda) \frac{e^{[\omega_n \xi - i(\omega_n \sqrt{1-\xi^2} - \lambda)]t_0}}{\omega_n \xi - i(\omega_n \sqrt{1-\xi^2} - \lambda)} d\lambda \\
 &= \frac{1}{2\pi} e^{\omega_n \xi t_0} e^{-i\omega_d t_0} \int_{-\infty}^{\infty} \frac{Z(\lambda) e^{i\lambda t_0}}{\omega_n \xi - i(\omega_n \sqrt{1-\xi^2} - \lambda)} d\lambda. \tag{18}
 \end{aligned}$$

Using Equation (15),

$$\eta_d^*(t_0) = \frac{1}{2\pi} e^{\omega_n \xi t_0} \int_{-\infty}^{\infty} \frac{Z(\lambda) e^{i\lambda t_0}}{\omega_n \xi - i(\omega_n \sqrt{1-\xi^2} - \lambda)} d\lambda + e^{i\omega_d t_0} \eta_{d_0}^* \tag{19}$$

But

$$\eta_d^*(t_0) = \dot{y} + i\omega_d y = (\dot{x} + \omega_n \xi x + i\omega_d x) e^{\omega_n \xi t} = \eta_d e^{\omega_n \xi t} \tag{20}$$

where

$$\eta_d = \dot{x} + \omega_n \xi x + i\omega_d x.$$

Equation (19) then gives

$$\eta_d(t_0) = \frac{1}{2\pi} \int_{-\infty}^{\infty} \frac{Z(\lambda) e^{i\lambda t_0}}{\omega_n \xi - i(\omega_n \sqrt{1-\xi^2} - \lambda)} d\lambda + e^{i\omega_n \sqrt{1-\xi^2} t_0} \eta_{d_0} e^{-\omega_n \xi t_0} \tag{21}$$

$$= X^*(\omega_d, \xi, t_0) + iY^*(\omega_d, \xi, t_0) + e^{i\omega_n \sqrt{1-\xi^2} t_0} \eta_{d_0} e^{-\omega_n \xi t_0} \tag{22}$$

where $X^*(\omega_d, \xi, t_0)$ and $Y^*(\omega_d, \xi, t_0)$ are the real and imaginary parts of the "Smoothed or Damped Fourier Transform" defined by the integral in

Equation (21). At the frequencies $\omega_d^m = \frac{2\pi m}{t_0}$

$$\eta_d(t_0) = X^*(\omega_d^m, \xi, t_0) + iY^*(\omega_d^m, \xi, t_0) + \eta_{d_0} e^{-\omega_n \xi t_0} \quad (23)$$

Simplifying Equation (23) we get

$$\left. \begin{aligned} x(\omega_d^m, \xi, t_0) &= \left(\frac{2\pi m}{t_0}\right)^{-1} Y^*(\omega_d^m, \xi, t_0) + x_0 e^{-\omega_n \xi t_0} \\ \dot{x}(\omega_d^m, \xi, t_0) &= X^*(\omega_d^m, \xi, t_0) - \beta Y^*(\omega_d^m, \xi, t_0) + \dot{x}_0 e^{-\omega_n \xi t_0} \end{aligned} \right\} \quad (24)$$

Equation (24) states that the pseudo-velocity of a damped oscillator with zero initial conditions having a damped natural frequency of ω_d^m and the fraction of critical damping, ξ , is given by the imaginary part of the smoothed Fourier transform evaluated at the frequency ω_d^m . Similar interpretations on the basis of the real part of the smoothed Fourier spectrum are possible. Lastly we observe that Equation (24) reduces to Equation (6) as $\xi \rightarrow 0$. When $X^* \equiv Y^* \equiv 0$, we have the free vibration problem of the damped oscillator indicating that the velocity and displacement of an oscillator at time t_0 (a complete multiple of $2\pi/\omega_d^m$) are respectively equal to the initial velocity and displacement multiplied by the factor $e^{-\omega_n \xi t_0}$.

The phase of the complex variable η_d is given by

$$\tan \varphi_d(t) = \left(\frac{\omega_n \sqrt{1 - \xi^2} x}{\dot{x} + \omega_n \xi x} \right) \quad (25)$$

When the oscillator starts from rest, for frequencies ω_d^m ,

$$\tan \varphi_d^m(t_0) = \frac{Y^*(\omega_d^m, \xi, t_0)}{X^*(\omega_d^m, \xi, t_0)} = \tan \psi_d(\omega_d^m, t_0) \quad (26)$$

where ψ_d is the phase of the smoothed Fourier transform of $\ddot{z}^*(t)$. Equations (25) and (26) are analogous to Equation (8) and (9). To study this analogy further we consider

$$\tan^2 \varphi_d = \frac{\omega_n^2(1-\xi^2)x^2}{\dot{x}^2 + 2x\dot{x}\xi\omega_n + \omega_n^2\xi^2x^2} \quad (27)$$

$$= \frac{kx^2 - k(\xi x)^2}{m\dot{x}^2 + c x\dot{x} + k(\xi x)^2} \quad (28)$$

Here k is the force per unit displacement of the spring and c is the viscous damping of the dashpot. As in Equation (8), the numerator of Equation (28) is related to the potential energy of an equivalent spring while the denominator is simply the total energy less the potential energy of the equivalent spring. The potential energy is reduced from the undamped case by a term $k(\xi x)^2$. This reduction may then be looked upon as being the cause of a reduced natural frequency in the damped system. The damping thus has the effect of reducing the apparent spring stiffness. Noting that $k(\xi x)^2 = (\frac{c^2}{4m})x^2 = k_1 x^2$, we observe that the dashpot can be interpreted as acting as a negative spring of stiffness $\frac{c^2}{4m}$. We then propose that the mass-spring-dashpot system can be looked upon as being composed of three different elements (Figure I.1(b)): an equivalent spring (I), a spring related to the damping characteristics of the dashpot (II), and a velocity dependent dissipative element (III). Element I, which represents the equivalent spring, yields the frequency characteristics of the system while element III yields the dissipative qualities associated with any oscillation of the mass m .

The parameter η_d then brings about a split-up of the energy which can be expressed through its phase angle as

$$\tan^2 \phi_d = \frac{(P.E.)_{\text{spring}} - (P.E.)_{\text{damper spring}'}}{(K.E.)_{\text{mass}} + (D.E.)_{\text{dashpot}} + (P.E.)_{\text{damper spring}'}}$$

When $\frac{c^2}{4m} = k$, the equivalent spring in the system has zero stiffness ($k_{eq} \equiv 0$), and an exponential decay sets in, thus leading to the concept of critical damping. For such an oscillator, the phase of the smoothed transform is identically zero for all frequencies ω_d^m and for all times t_0 .

The complex number η_d can be looked upon as a vector whose magnitude equals $\sqrt{e_d}$ while its phase angle is given by Equation (25). Thus

$$\eta_d = \sqrt{e_d} \exp(i\phi_d) \quad (29)$$

e_d is a positive definite quantity and is given by

$$e_d = \dot{x}^2 + \omega_n^2 x^2 + 2\omega_n \xi x \dot{x} = 2(K.E. + P.E. + D.E.) / m,$$

where K.E. represents the kinetic energy, P.E. the potential energy, and D.E. the damping energy. The rate of rotation of this vector can be derived in a form similar to that of Equation (13).

$$\frac{d\phi_d}{dt} = \omega_d \left[1 + \frac{x\ddot{x}}{e_d} \right] \quad (30)$$

For the free vibration case $\frac{d\phi_d}{dt} = \omega_d$, the damped natural frequency of vibration.

Just as the Fourier transform gave the response (η) of an undamped oscillator at the end of the excitation, t_0 , so also the damped Fourier transform ($X^* + iY^*$) yields the response of a damped oscillator (η_d) at time t_0 . The velocity spectrum $S_v(\omega_n, \xi)$ can again be defined as $|\eta_d|_{\max} = |\dot{x} + \beta\omega_d x + i\omega_d x|_{\max}$ for the damped case.

Equation (21) indicates that the damped Fourier spectral amplitude cannot be directly obtained from the Fourier spectral amplitudes by the use of a simple linear filtering operation performed on the Fourier spectrum. This damped spectral amplitude for any particular damping $\xi = \xi_0$ computed at the end of the excitation will serve as a lower bound on the damped ($\xi = \xi_0$) velocity spectrum for an oscillator with natural frequency ω_n and percentage of critical damping, ξ . The damped Fourier spectrum, $F_d = X(\omega_d, \xi, t_0) + iY(\omega_d, \xi, t_0)$ is a lower bound on the damped relative velocity spectrum $S_v(\xi, \omega_n)$.

Calculation of the Damped Fourier Spectrum (D. F. S.)

The damped Fourier spectrum $F_d(\omega_d, \xi, t_0)$ is defined (refer to Equation 21) as

$$F_d(\omega_d, \xi, t_0) = \frac{1}{2\pi} \int_{-\infty}^{\infty} \frac{Z(\lambda) e^{i\lambda t_0} d\lambda}{\omega_n \xi - i(\omega_n \sqrt{1 - \xi^2} - \lambda)}. \quad (31)$$

Physically, Equation (29) implies that the response of a damped oscillator at any time t_0 to a given excitation can be obtained if a knowledge of the response at time t_0 (to that excitation) of undamped oscillators of all possible frequencies is known. Since the calculation of $Z(\lambda)$ is generally done using the Fast Fourier Transform (F. F. T.) its values are known only at $\lambda = \frac{2\pi n}{t_0}$ $n = 0, 1, \dots$. Hence $Z(\lambda)$ needs to be reconstructed for intermediate frequencies between these discrete values using the sampling theorem.

$$Z(\omega) = \sum_{n=-\infty}^{\infty} Z\left(\frac{2\pi n}{t_0}\right) e^{-\frac{i\omega t_0}{2}} e^{in\pi} \frac{\sin\left(\frac{\omega t_0}{2} - n\pi\right)}{\left(\frac{\omega t_0}{2} - n\pi\right)}.$$

Then

$$\begin{aligned}
 F_d &= \frac{1}{2\pi} \int_{-\infty}^{\infty} \sum_{n=-\infty}^{\infty} Z\left(\frac{2n\pi}{t_0}\right) e^{-\frac{i\omega t_0}{2}} e^{in\pi \frac{\sin\left(\frac{\omega t_0}{2} - n\pi\right)}{\left(\frac{\omega t_0}{2} - n\pi\right)}} \frac{e^{i\omega t_0} d\omega}{\left(\omega_n \xi - i\left(\omega_n \sqrt{1-\xi^2} - \omega\right)\right)} \\
 &= \frac{1}{2\pi} \sum_{n=-N}^N Z\left(\frac{2n\pi}{t_0}\right) \int_{-\infty}^{\infty} \frac{\sin\left(\frac{\omega t_0}{2} - n\pi\right)}{\left(\frac{\omega t_0}{2} - n\pi\right)} \frac{e^{\frac{i\omega t_0}{2}} d\omega}{\left(\omega_n \xi - i\left(\omega_n \sqrt{1-\xi^2} - \omega\right)\right)} \\
 &= \frac{1}{t_0} \sum_{n=-N}^N Z\left(\frac{2n\pi}{t_0}\right) \frac{1 - e^{-\left(\omega_n \xi - i\omega_n \sqrt{1-\xi^2}\right)t_0}}{\omega_n \xi - i\left(\omega_n \sqrt{1-\xi^2} - \frac{2n\pi}{t_0}\right)}.
 \end{aligned}$$

If further $\omega_n = \frac{2\pi m}{t_0}$,

$$F_d(\omega_d^m, \xi, t_0) = \sum_{n=-N}^N Z\left(\frac{2n\pi}{t_0}\right) \left[\frac{1 - e^{-2\pi m (\xi - i\sqrt{1-\xi^2})}}{2\pi m \xi - i2\pi (m\sqrt{1-\xi^2} - n)} \right]. \quad (32)$$

The interchange of summation with integration can be justified on the grounds that the signal is almost frequency band limited.

Though the summation in Equation (32) does not represent a simple convolution, it is done on a product of $Z(\lambda)$ and a sharply peaked function so that the actual summation may be truncated to a smaller number of frequency estimates around the frequency of interest. This is what one would actually expect, for at a given frequency the damped Fourier amplitude spectrum ought to depend more closely on the Fourier spectral amplitude at that and neighboring frequencies.

To illustrate the concept of the damped spectrum, three accelerograms were analyzed. They are shown in Figures I.2(a), (b) and (c). The spectrum curves corresponding to these three acceleration time histories for various

EUREKA EARTHQUAKE, DEC 21, 1954
N11W COMPONENT OF ACCELERATION

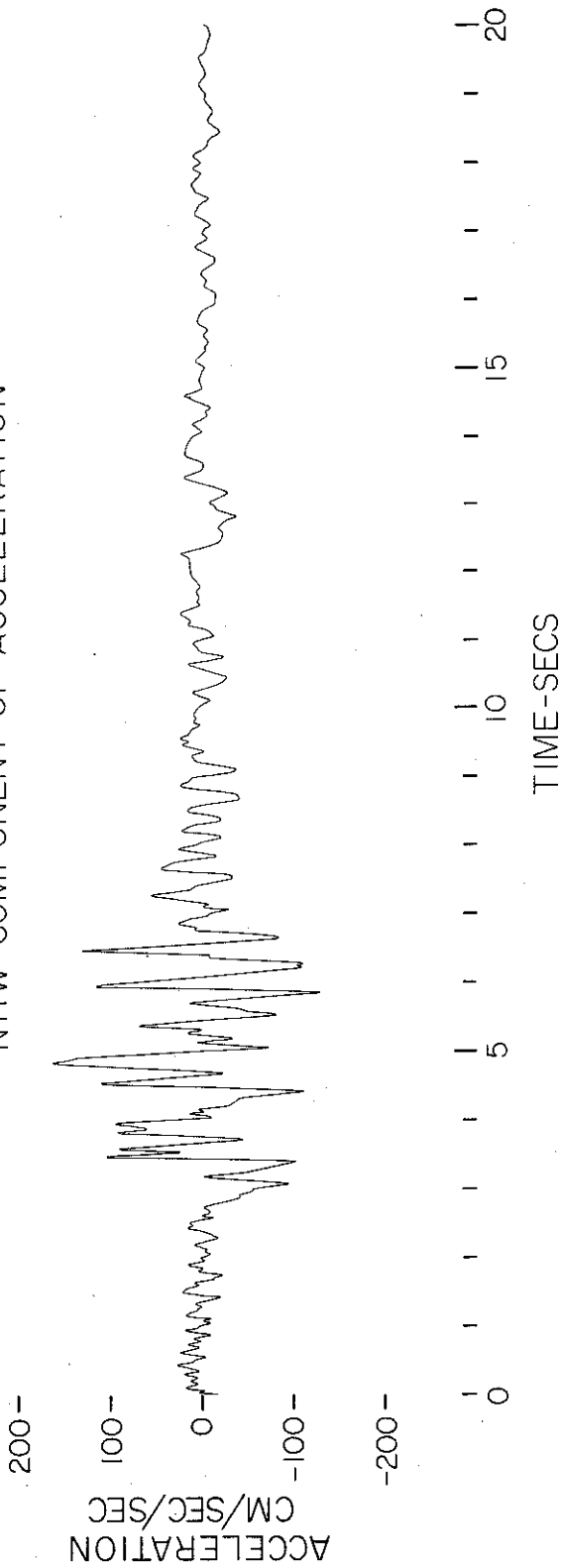


Figure I. 2 (a) Acceleration-time history of the Eureka Earthquake Record, indicating a short burst of energy.

IMPERIAL VALLEY EARTHQUAKE, MAY 18, 1940
S90W COMPONENT OF ACCELERATION

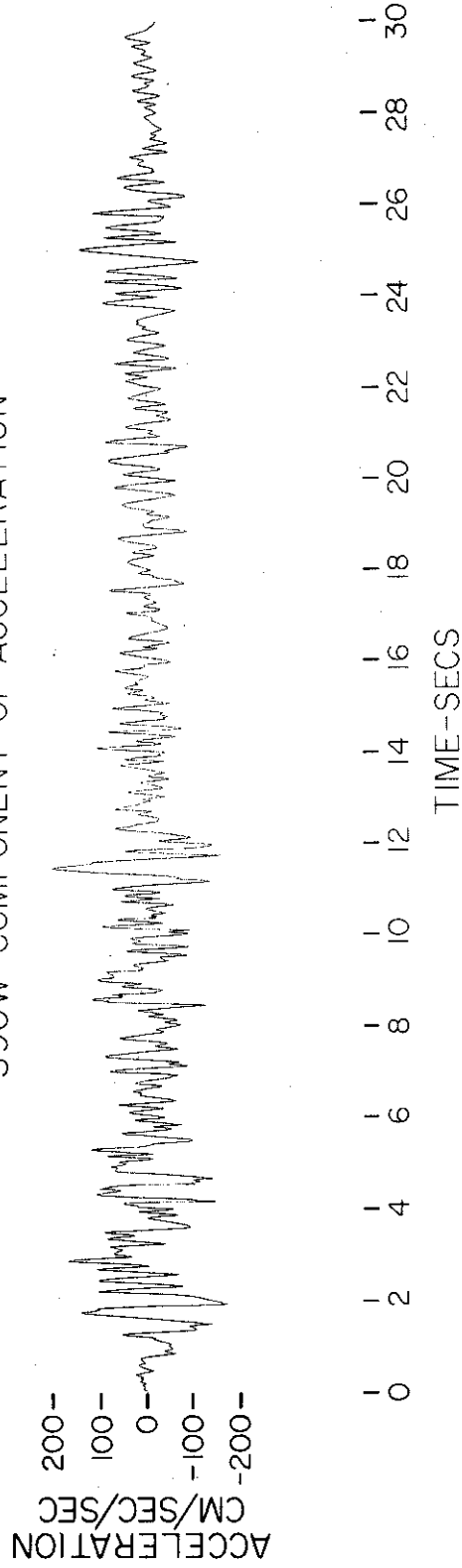


Figure I. 2 (b) Acceleration-time history of the El Centro event of 1940 indicating a nearly stationary type of excitation.

KERN COUNTY EARTHQUAKE, JULY 21, 1954
VERTICAL COMPONENT OF ACCELERATION

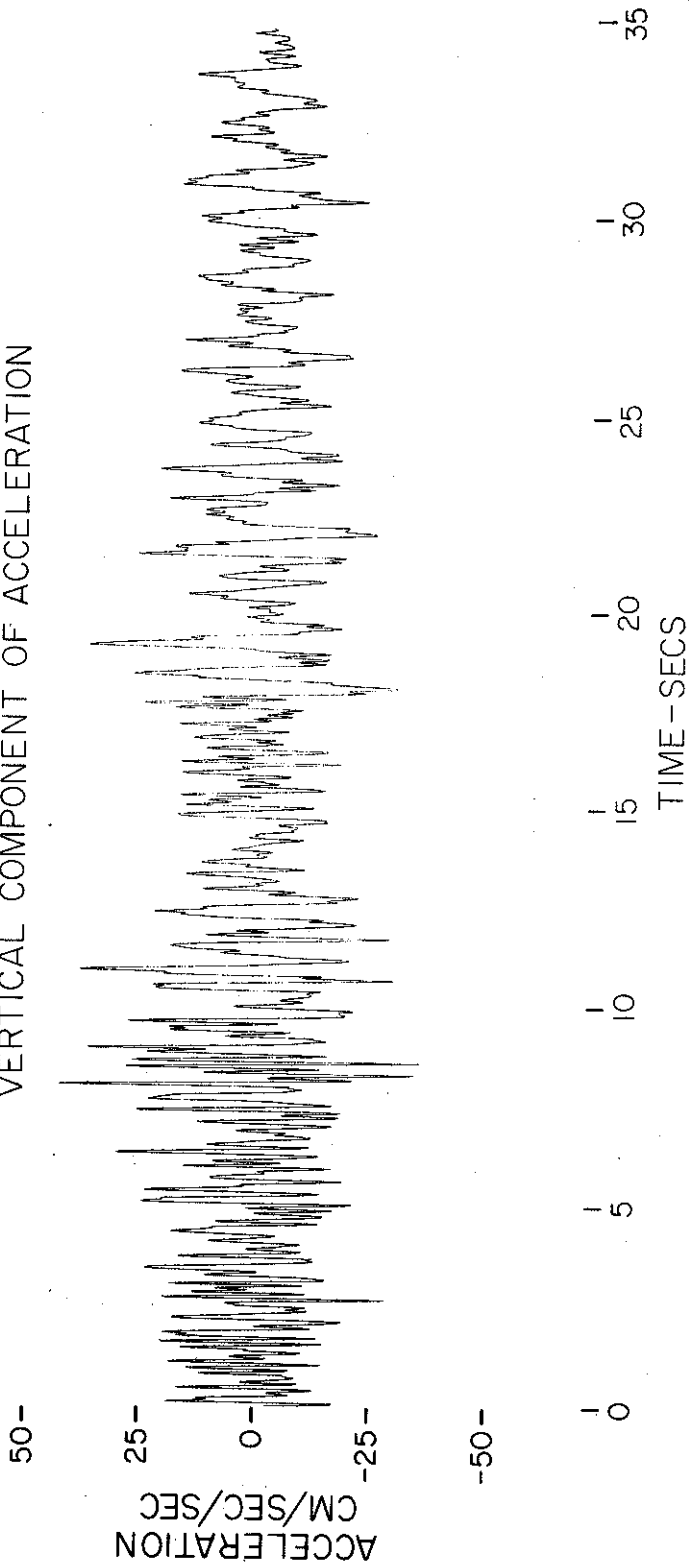


Figure I. 2 (c) Acceleration-time history of the Kern County accelerogram showing a clearly non-stationary character, the contributions from higher frequencies becoming relatively small beyond about twenty seconds.

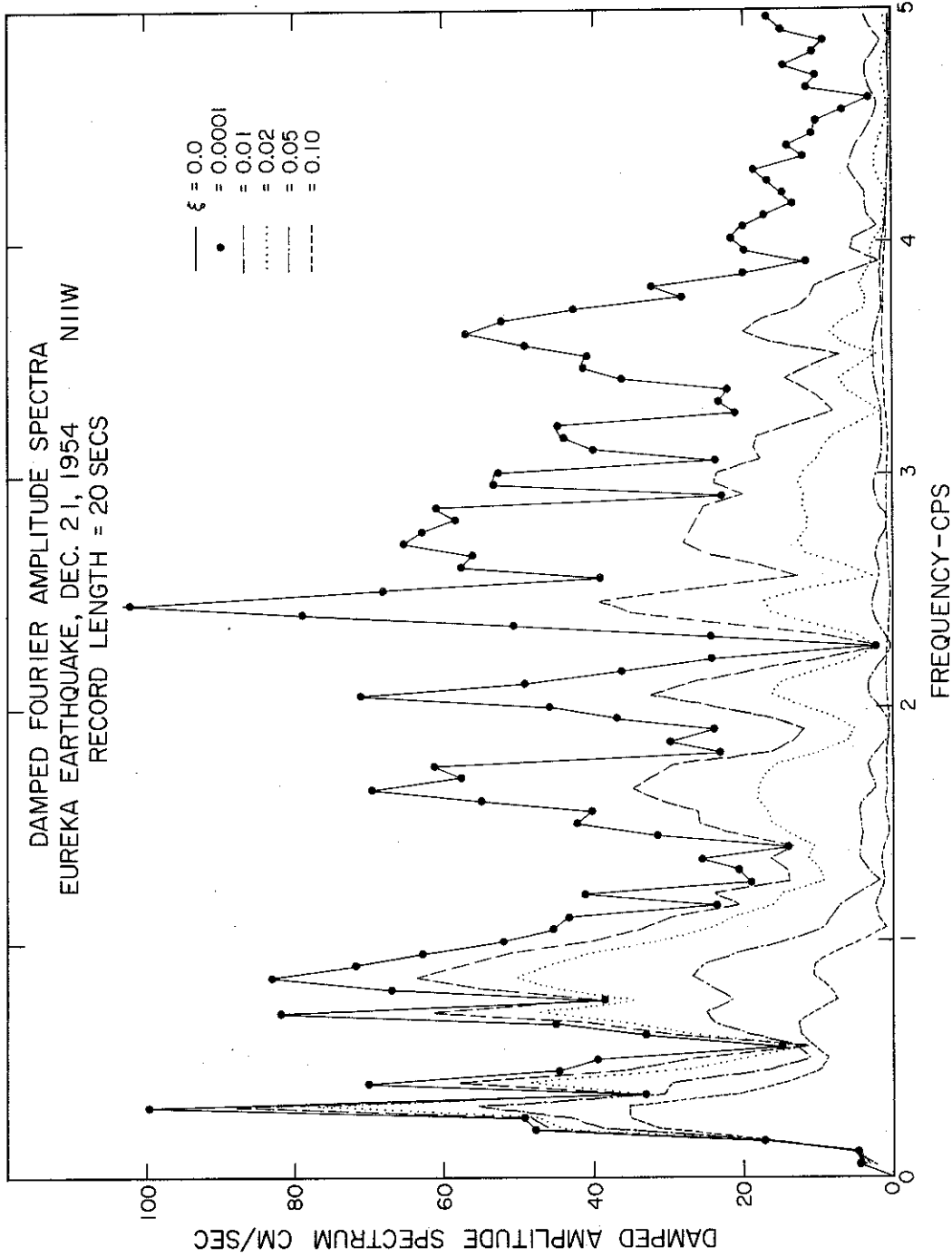


Figure I. 3 Damped Fourier amplitude spectrum curves.

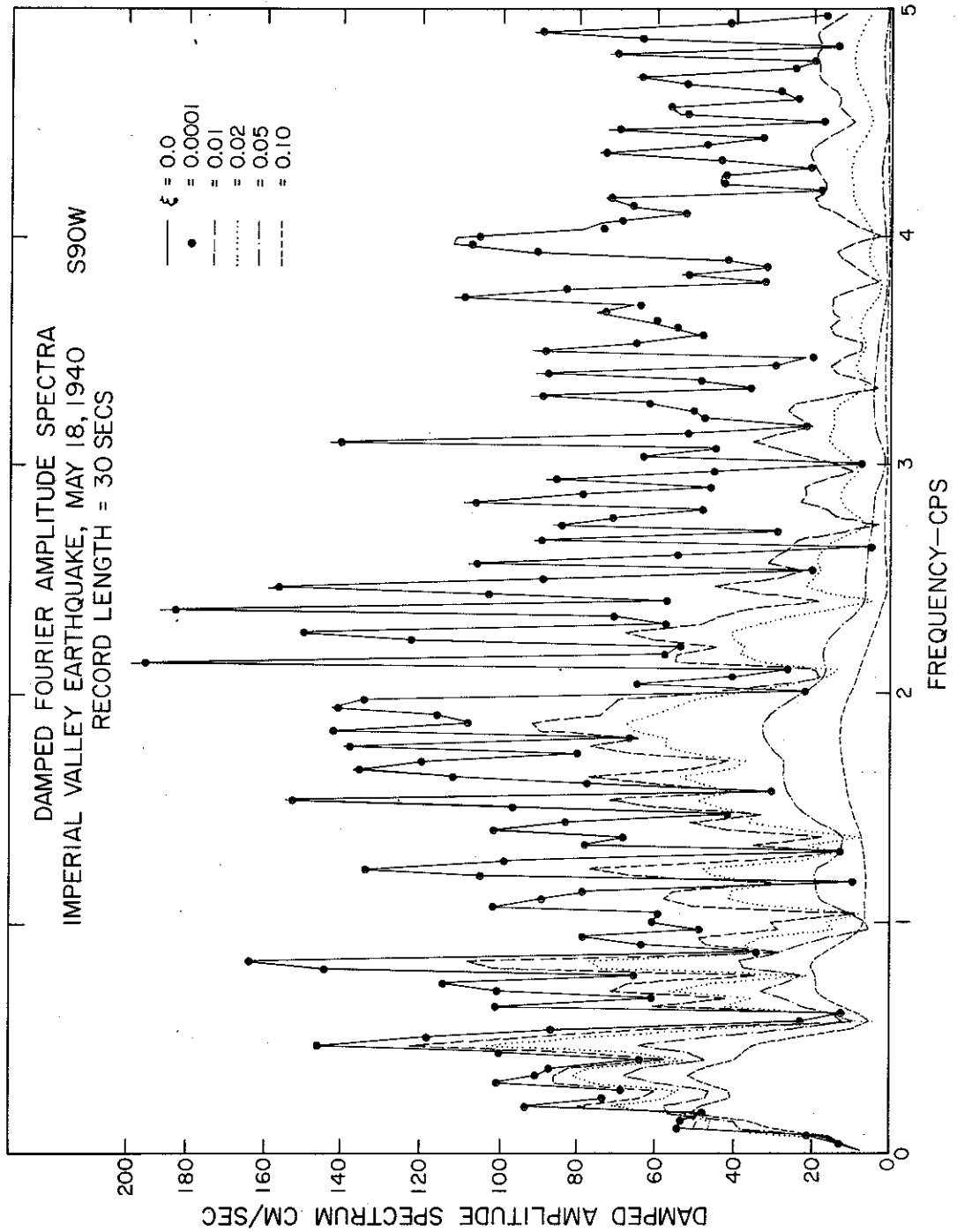


Figure I. 4 Damped Fourier amplitude spectrum curves.

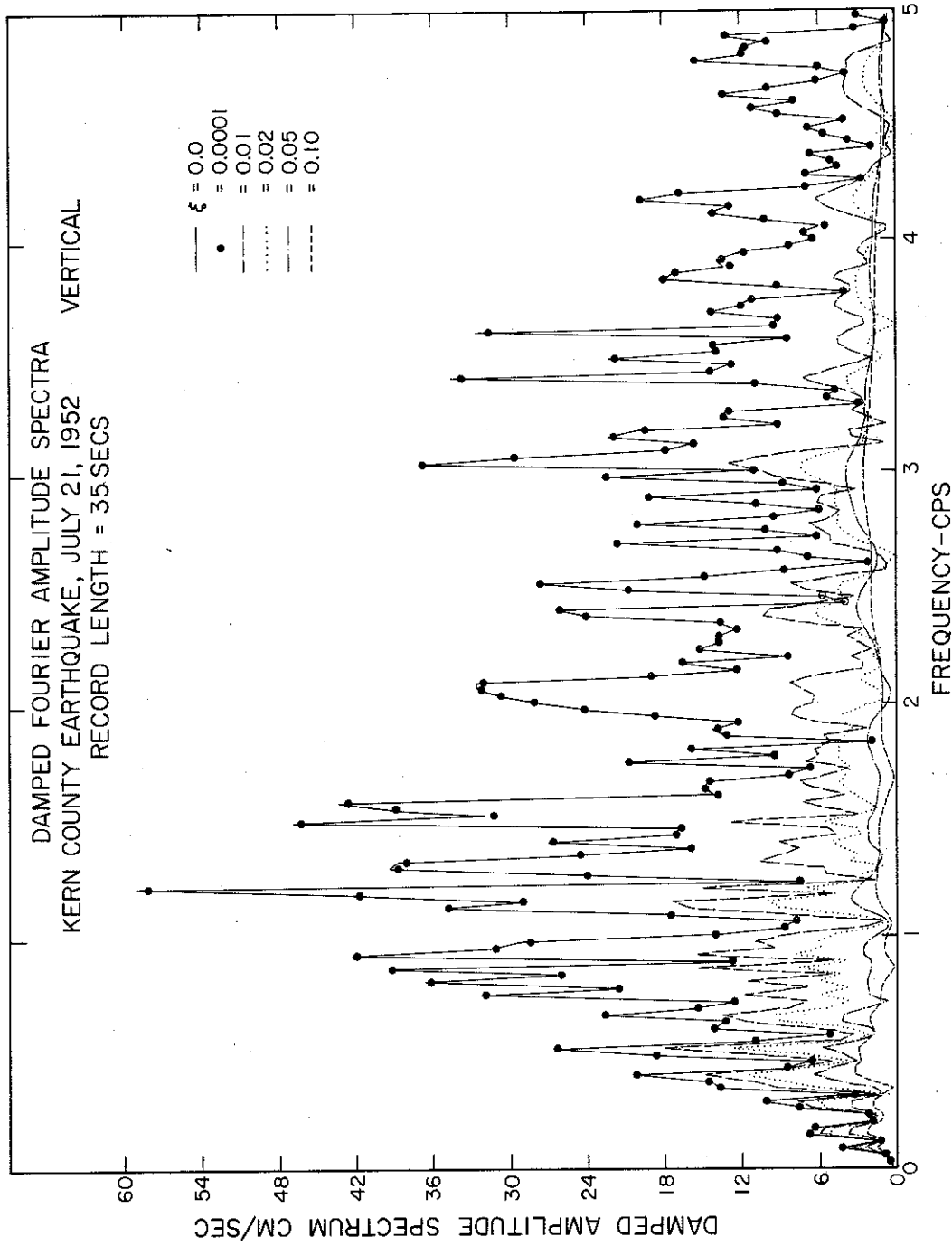


Figure I. 5 Damped Fourier amplitude spectrum curves.

values of ξ are shown in Figures I. 3, I. 4 and I. 5. The spectra have been obtained by taking 500 frequency estimates of the Fourier spectrum around the frequency of interest.

The exponential decay of the damped oscillator leads to low responses at higher frequencies, thereby quite appreciably reducing the spectral amplitudes beyond about 2 cps. The upper solid curves in Figures 2 and 3 are the Fourier amplitude spectrum, while the full circles indicate the damped spectrum estimates for a damping value of .01%. We observe that these points lie below the spectrum curve, though they follow it closely. As seen from the figures, the effect of damping on the response as indicated by the damped spectral amplitudes is quite intense. For damping values as low as 1%, the spectral amplitudes are reduced by about half to a third of those obtained from the undamped spectra. It may be noted that the spectral curves for various damping occasionally cross each other and that the curves for higher ξ values show lesser undulations so that the introduction of damping in this way effects a kind of smoothing.

On the Smoothing of Fourier Amplitude Spectra

Various investigators^(5,6,7,8) have looked at the problem of smoothing of spectra from the point of view of time series analyses. Most smoothing operators suggested are linear. They show no preference for any range of frequencies and are so manipulated as to keep the area under the smoothed curves identical to the area under the unsmoothed curves. As observed from the damped spectra, the operation represented by the integral in Equation (21) could be referred to as a smoothing operation that yields smoother spectral curves (Figures I.3, I.4 and I.5). However, there are some marked differences between this operation and the smoothing

operators that have been suggested by workers in time series analysis. Firstly, it is impossible to convert Equation (21) into the classical convolution integral. The higher frequencies are modulated to a greater extent than lower frequencies. Secondly, the areas under the smoothed curves are not identical to those under the unsmoothed curves. These two results fall out naturally when we consider the fact that every point on the smoothed Fourier spectrum curve corresponds to the response of a damped oscillator which decays as $e^{-\omega_n \xi t}$, so that the higher frequencies become attenuated to a greater extent. The dissipation of energy through the dashpot in the damped system causes the area under the smoothed and unsmoothed curves to be different.

This effect can be best illustrated through a simple example as follows. Let $\ddot{z}(t) = \delta(t)$, so that $Z(\lambda) = 1$. Then,

$$F_d = \dot{x} + \omega_n \xi x + i\omega_d x \Big|_{t=t_0} = \frac{1}{2\pi} \int_{-\infty}^{\infty} \frac{Z(\lambda) e^{i\lambda t_0} d\lambda}{\omega_n \xi - i(\omega_n \sqrt{1 - \xi^2} - \lambda)} \quad (33)$$

Integrating we get

$$F_d = e^{i\omega_n \sqrt{1 - \xi^2} t_0} e^{-\omega_n \xi t_0} \quad (34)$$

$$|F_d| = e^{-\omega_n \xi t_0} \quad (35)$$

But, $|Z(\omega_n, t_0)|$ is the energy of an undamped oscillator caused to oscillate by the delta function pulse (see Eq. 12). Also, $|F(\omega_d, t_0)|$ is the energy of a damped oscillator. We observe that this energy, unlike in the undamped case, is a function of the frequency and the time duration t_0 . In this case, the unsmoothed and the smoothed spectra would be represented as in Figure I.6. The damped curves represent the response at time $t=t_0$ of an oscillator of natural

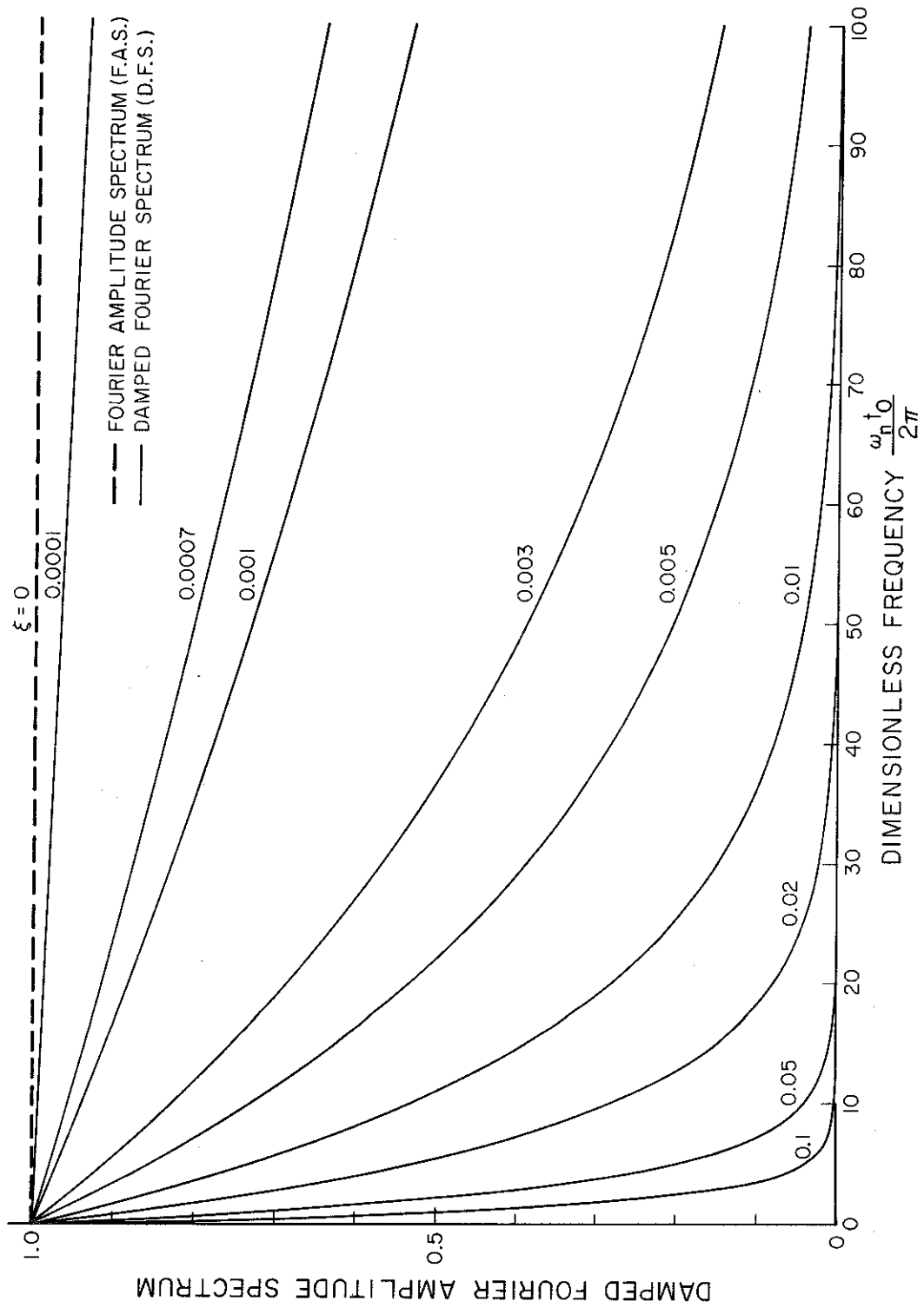


Figure I. 6 Damped Fourier amplitude spectrum curves indicating the response $|F_d|$ of an oscillator of natural frequency ω_n and percentage of critical damping, ξ , to a delta function input at time $t=0$.

frequency ω_n and damping ξ to a delta function applied at time $t=0$. The nondimensional frequency clearly indicates that for a given damping value, the response at larger times (t_0) for smaller natural frequencies (ω_n) will be the same as the response at shorter times at higher frequencies provided the product $\omega_n t_0$ is the same. As observed from Figure I.6, at higher frequencies the damped oscillator shows a very short memory of past excitation.

Accelerograms are far from ergodic since they generally represent bursts of energy arriving with the various wave phases. The response of a heavily damped oscillator which has a rather short lived memory tends to follow these bursts of energy. The longer memory (theoretically ∞) of an undamped oscillator generally leads to a response which does not fluctuate so much in time, the oscillator trying, as it were, to compensate for the short durations of lower level excitations which occur between successive energy bursts, by utilizing its memory of larger past motions. This observation would be useful in understanding some aspects of the analyses presented in Part II.

II. STATISTICAL DISTRIBUTION OF THE MAXIMA OF A RANDOM FUNCTION WITH APPLICATIONS TO RESPONSE SPECTRUM ANALYSES

Introduction

The purpose of this section is to summarize some of the well-known results in the theory of random functions and to use those results

in the interpretation of response spectra. The specific properties of random functions which will be of most interest in this context are related to the distribution of extreme values, the expected values of the maxima in a given interval of time, and the relationship of these maxima to the root-mean-square value of the same function. It is through these relationships that it will be possible to relate the response spectrum and Fourier amplitude spectrum curves in the most physically meaningful way to the extreme value statistics of the problem.

Strong earthquake ground motion is, of course, not an ergodic process in time^(9, 10, 11), and consequently, the response of an oscillator to such an input is likewise not ergodic. Many earthquake records show slowly dying-out tails leading to responses, in particular of damped systems (which do not for all practical purposes have infinite memory) that may be far from ergodic. In order to highlight the possible relationship between the Fourier amplitude spectrum and the extreme values of the oscillator response, as a first approximation we will assume that the response may be described approximately by the theory of random ergodic processes.

Though the results of this section can be extended to functions as $\ddot{z}(t) = e(t) s(t)$ where $e(t)$ is the envelope function of the ergodic process $s(t)$, the main objective here is to explore the nature of the above-mentioned relationships from a qualitative and physical point of view. It is felt that such an assumption, though strictly invalid, may lead us to a better understanding of the nature of structural response.

The Distribution of Maxima of a Random Function

The random function of time, $f(t)$, shown in Figure II.1, can represent, for example, the response of an oscillator to the earthquake ground motion. Following Cartwright and Longuet-Higgins⁽¹²⁾, $f(t)$ may be represented as the sum of an infinite number of sine waves

$$f(t) = \sum_n c_n \cos(\omega_n t + \varphi_n) \quad (1)$$

with frequencies ω_n distributed densely in the interval $(0, \infty)$. The phases φ_n are assumed to be random and uniformly distributed between 0 and 2π . $E(\omega)$, the energy spectrum of $f(t)$, is related to the amplitudes c_n through

$$\sum_{\omega_n = \omega}^{\omega + d\omega} \frac{1}{2} c_n^2 = E(\omega) d\omega \quad (2)$$

The total energy per unit length of the record, corresponding to the first moment of $E(\omega)$ about the origin, is

$$m_0 = \int_0^{\infty} E(\omega) d\omega \quad (3)$$

while the n^{th} moment is defined by

$$m_n = \int_0^{\infty} E(\omega) \omega^n d\omega \quad (4)$$

Detailed analysis of the statistical distribution of the maxima of $f(t)$ ^(12, 13) show that this distribution depends on only two parameters: the root-mean-square value of $f(t)$, $m_0^{1/2}$, and a parameter ϵ measuring the relative width of the frequency spectrum $E(\omega)$, and defined by

$$\epsilon^2 = 1 - \frac{m_2^2}{m_0 m_4} \quad (5)$$

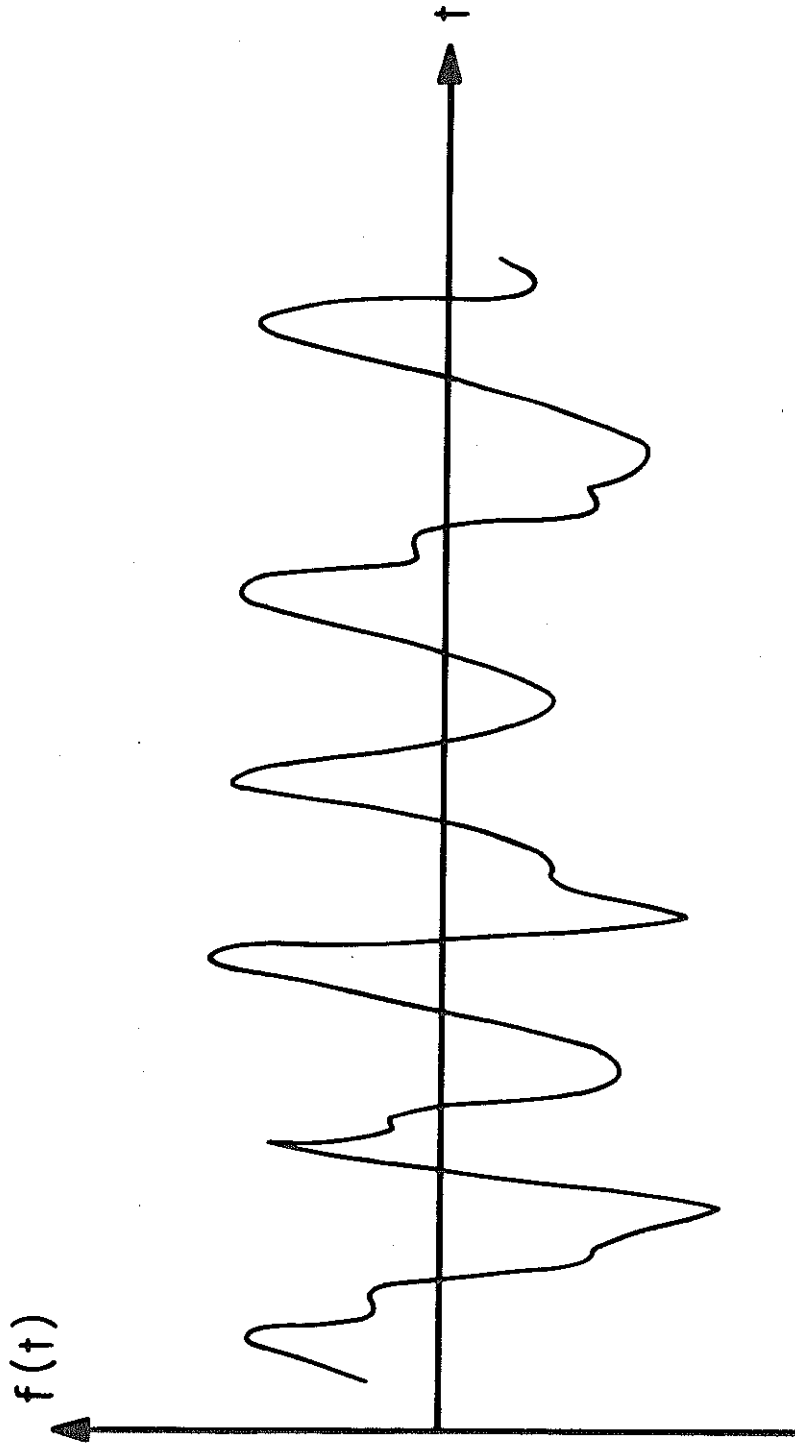


Figure II. 1 A typical random function $f(t)$.

From the Cauchy-Schwartz inequality, ϵ cannot be imaginary.

After normalizing $f(t)$ by

$$f(t)/m_0^{1/2} = \eta \quad (6)$$

the probability distribution of the heights of the maxima of $f(t)/m_0^{1/2}$ becomes⁽¹²⁾

$$p(\eta) = \frac{1}{(2\pi)^{1/2}} \left[\epsilon e^{-\frac{1}{2} \frac{\eta^2}{\epsilon^2}} + (1 - \epsilon^2)^{1/2} \eta e^{-\frac{1}{2} \eta^2} \int_{-\infty}^{\eta \frac{(1 - \epsilon^2)^{1/2}}{\epsilon}} e^{-\frac{1}{2} x^2} dx \right] \quad (7)$$

and is shown in Figure II.2. The statistical distribution of the minima is the reflection of (7) in the mean level $\eta = 0$.

Physically, the parameter ϵ is a measure of the relative proportions of the various frequencies contained in a signal. To fix our ideas on this parameter, let us determine values for the three energy spectra indicated in Figures II.3a, b, c. Figure II.3a indicates the spectrum of a pure sine wave. The values of the zeroth, second and fourth moments are a , $a\omega_0^2$ and $a\omega_0^4$ so that $\epsilon = 0$. The corresponding distribution given by Equation (7) then reduces to

$$p(\eta) = \begin{cases} \eta e^{\frac{1}{2} \eta^2} & \eta \geq 0 \\ 0 & \eta \leq 0 \end{cases} \quad (8)$$

showing that for an infinitely narrow spectrum, $p(\eta)$ becomes a Rayleigh distribution.

For the rectangular block shown in Figure II.3b, $\epsilon = 2/3$. The flat nature of the spectrum is indicative of equal proportions of high and low frequency contents. Figure II.3c indicates two delta functions at frequencies ω_0 and $\delta\omega_0$ of strengths a and $b(=\beta a)$. For such a spectrum,

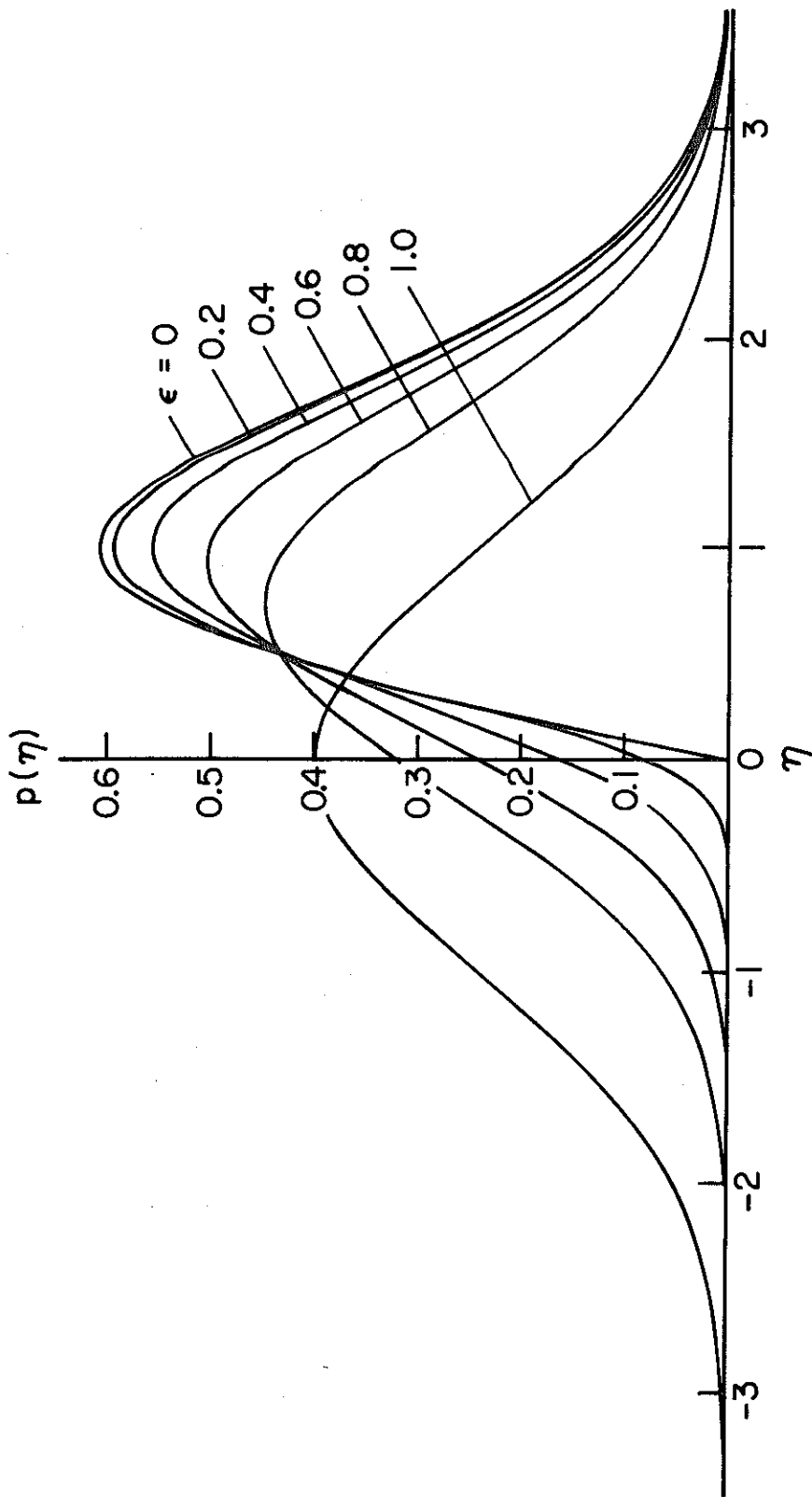


Figure II. 2 Graphs of $p(\eta)$, the probability distribution of the heights of maxima for various values of ϵ .

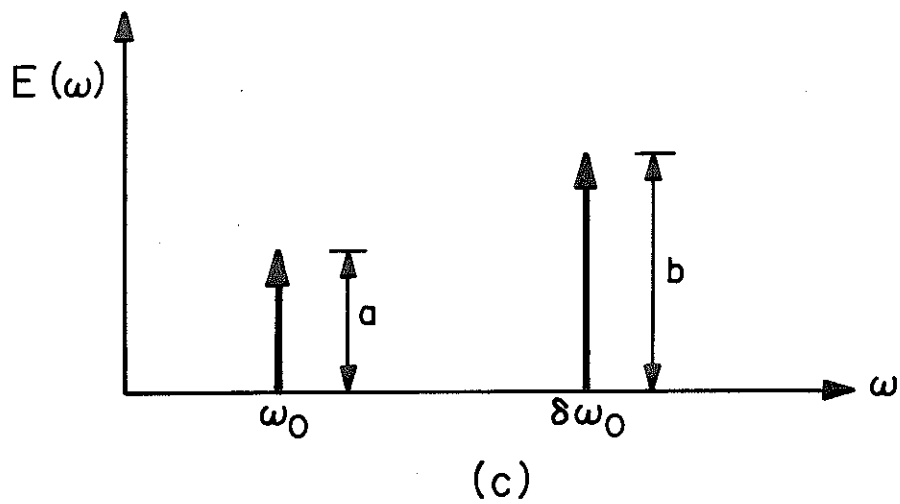
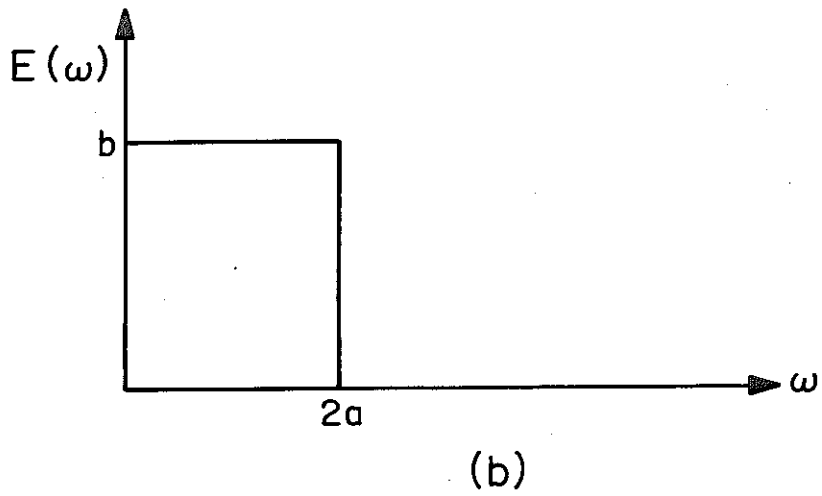
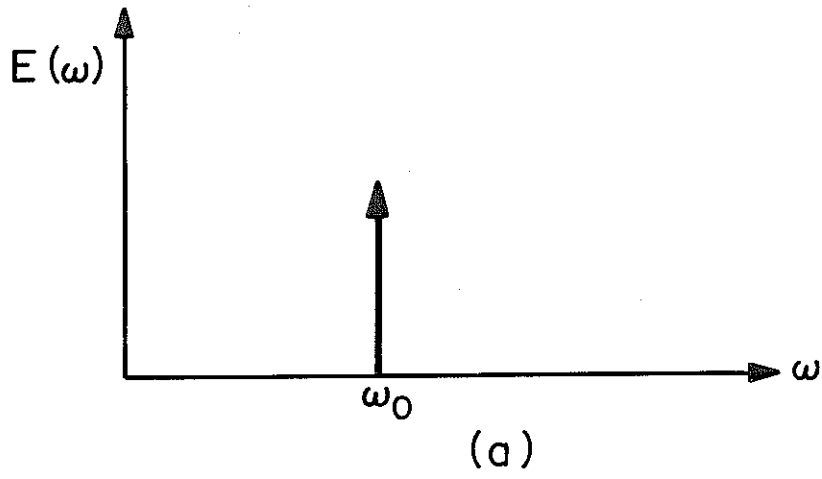


Figure II. 3 Three types of energy spectra illustrating the dependence of ϵ on the shape of the power spectrum.

$$\epsilon^2 = 1 - \frac{(1 + \delta^2 \beta)^2}{(1 + \beta)(1 + \delta^4 \beta)}$$

the value of ϵ depends on the relative strengths of the two waves together with their frequency separation. For a fixed $\delta = \delta_0$, if $\beta \rightarrow 0$, or $\beta \rightarrow \infty$, $\epsilon \rightarrow 0$ and we get the single sine wave case. When, for example, $\delta \rightarrow 1/\beta^{1/2}$ and $\beta \rightarrow 0$, $\epsilon \rightarrow 1$ thereby indicating a shift towards a Gaussian distribution. The distribution of maxima tends to the distribution of $f(t)/m_0^{1/2}$. In this case, we might expect equal number of positive and negative maxima of $f(t)/m_0^{1/2}$ and therefore a $p(\eta)$ symmetric about $\eta = 0$. Indeed, setting $\epsilon = 1$ in (7) we obtain

$$p(\eta) = \frac{1}{(2\pi)^{1/2}} e^{-\frac{1}{2}\eta^2} \quad (9)$$

which is the Gaussian distribution. For values of ϵ between 0 and 1, $p(\eta)$ lies between the Rayleigh and Gaussian distributions as shown in Figure II.2.

A typical example in Figure II.4 illustrates how ϵ measures the relative width of the power spectrum of the response of a single degree of freedom system to a stationary excitation having a power spectrum as given by

$$\Phi(\omega) = \frac{1}{1 + \left(\frac{\omega}{\alpha}\right)^2} \quad (10)$$

The transfer function of the single degree of freedom system is given by

$$H(\omega) = \frac{1}{\omega_n^2 - \omega^2 - 2i\omega_n \zeta \omega} \quad (11)$$

The dimensionless parameter

$$\zeta = \frac{\alpha}{\omega_n} \quad (12)$$

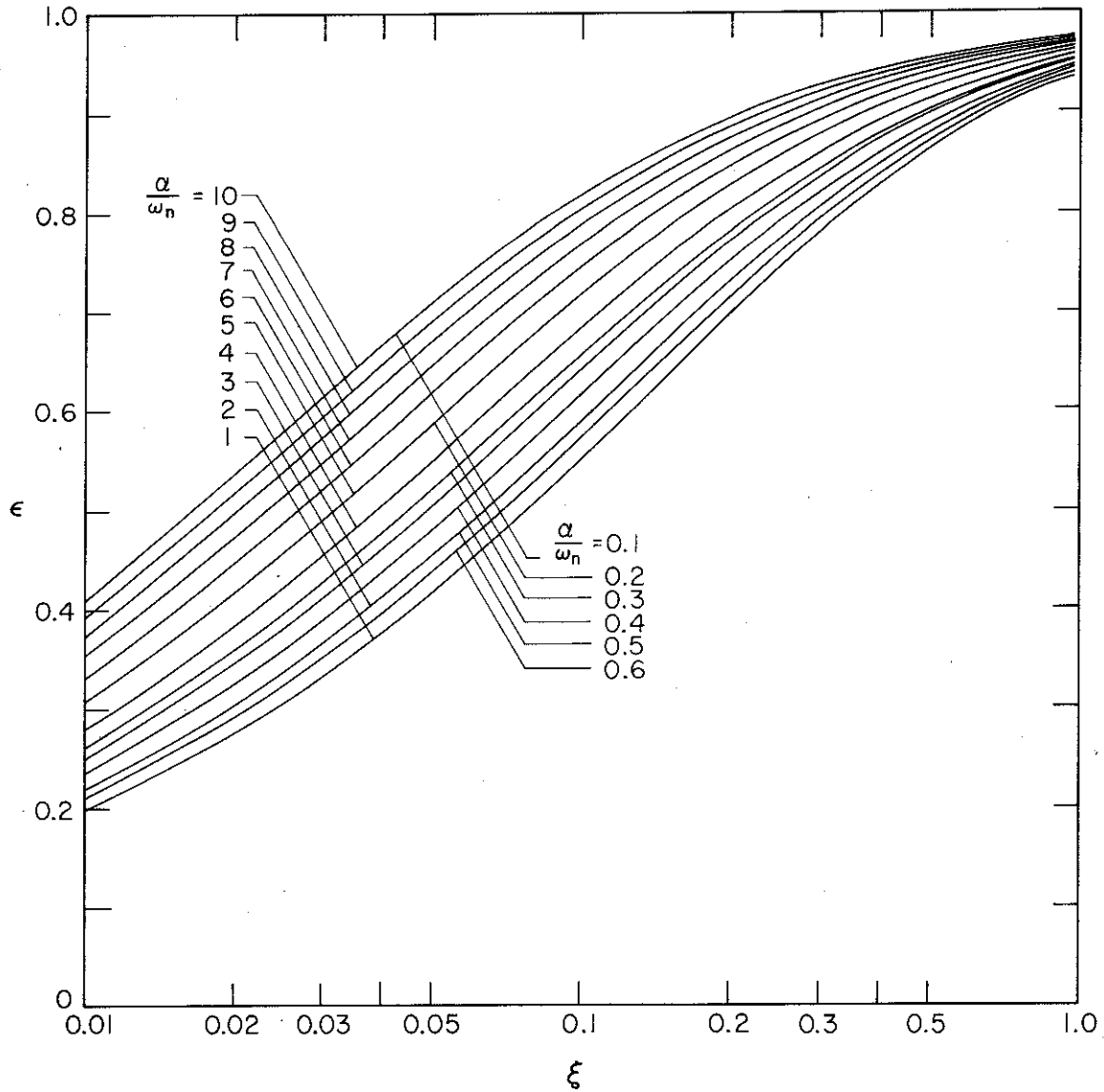


Figure II. 4 Graph of ϵ as a function of the percentage of critical damping, ξ , of a single degree of freedom system subjected to the band limited (from 0 to α radians/sec) signal $\Phi(\omega)$.

is a measure of the width of the input spectrum relative to the natural frequency of the oscillator considered. Figure II.4 then shows that when ξ , the fraction of critical damping, tends to zero, i. e., when the peak of the transfer function $H(\omega)$ at $\omega=\omega_n$ becomes sharper and higher, the oscillator becomes increasingly more sensitive only to the input frequencies $\omega \approx \omega_n$ and the output spectrum reduces to a narrow band centered at $\omega=\omega_n$ with $\epsilon \ll 1$. In the other extreme case, when $\xi \rightarrow 1$ the oscillator "feels" all frequencies between 0 and ω_n equally well, the output spectrum broadens and $\epsilon \rightarrow 1$. In addition to this effect of ξ , the influence of the cut-off frequency $\alpha = \zeta \omega_n$ of the input spectrum on ϵ , also shown in Figure II.4, demonstrates that for the broad band excitation only small ξ leads to a "narrow" output spectrum as measured by ϵ .

The probability $q(\eta)$ of η exceeding a given value is given by

$$q(\eta) = \int_{\eta}^{\infty} p(\eta) d\eta \quad (13)$$

Using (7) and (13) it can be shown (12) that

$$q(\eta) = \frac{1}{(2\pi)^{\frac{1}{2}}} \left[\int_{\eta/\epsilon}^{\infty} e^{-\frac{1}{2}x^2} dx + (1 - \epsilon^2)^{\frac{1}{2}} e^{-\frac{1}{2}\eta^2} \int_{-\infty}^{\eta \frac{(1 - \epsilon^2)^{\frac{1}{2}}}{\epsilon}} e^{-\frac{1}{2}x^2} dx \right] \quad (14)$$

For the Rayleigh distribution of peaks of $f(t)/m_0^{1/2}$ corresponding to $\epsilon = 0$

$$q(\eta) = \begin{cases} 1 & \eta \leq 0 \\ e^{-\frac{1}{2}\eta^2} & \eta \geq 0 \end{cases} \quad (15)$$

while for the Gaussian distribution of peaks ($\epsilon = 1$)

$$q(\eta) = \frac{1}{(2\pi)^{\frac{1}{2}} \eta} \int_{\eta}^{\infty} e^{-\frac{1}{2}x^2} dx \quad (16)$$

The curves of $q(\eta)$ for $\epsilon = 0, 0.2, 0.4, 0.6, 0.8$ and 1 are shown in Figure II.5.

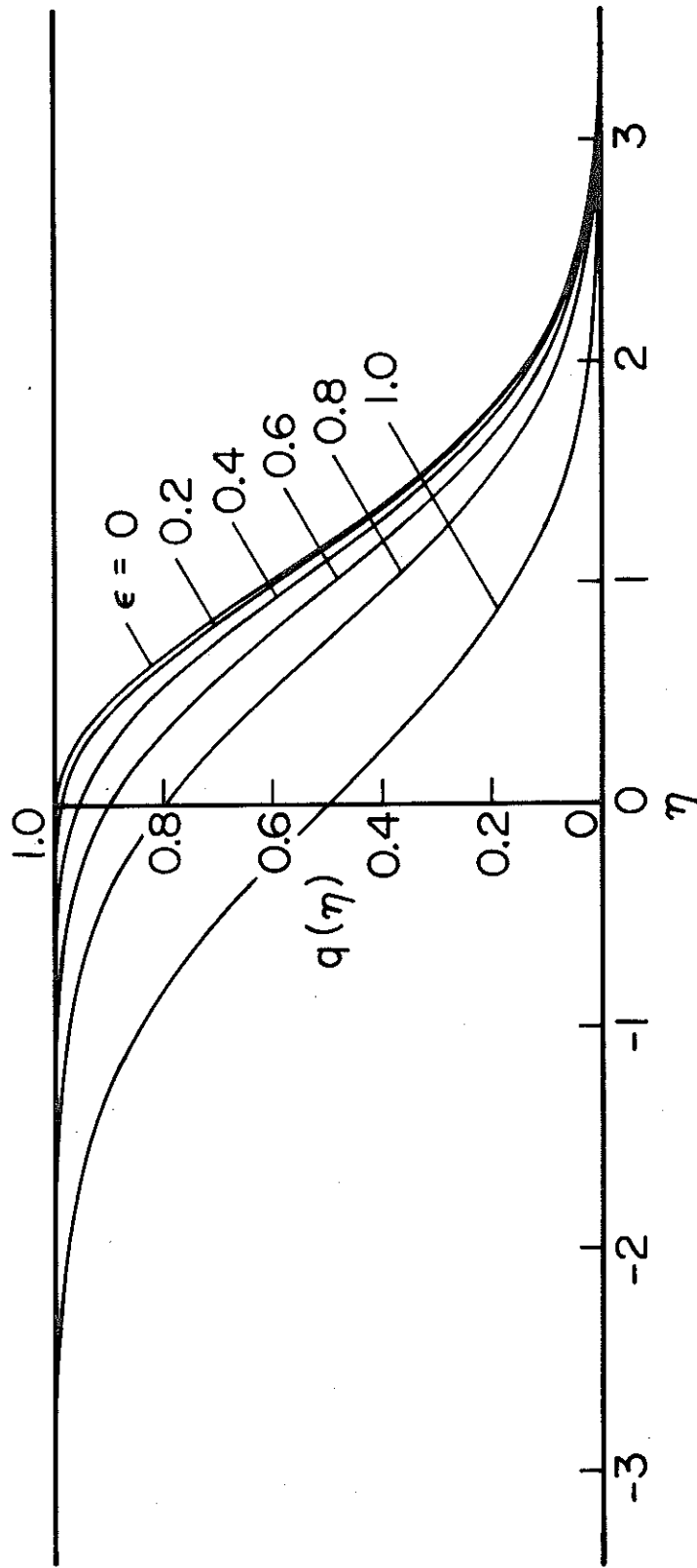


Figure II. 5 Graphs of the cumulative probability $q(\eta)$ for various ϵ values.

Functions with Narrow Frequency Band

The root-mean-square amplitude of successive peaks of $f(t)$, having a narrow power spectrum and centered at ω_0 , will now be considered. We denote the peaks of $f(t)$ by $a_1, a_2, \dots, a_{n-1}, a_n$ in the interval of time $N\tau/2$, where the interval between the successive crests is approximately equal to $\tau = 2\pi/\omega_0$ (Figure II.6). The root-mean-square of the peak amplitudes, \bar{a} , is then defined by

$$\bar{a} = \left\{ \frac{1}{N} (a_1^2 + a_2^2 + \dots + a_N^2) \right\}^{\frac{1}{2}} \quad (17)$$

The root-mean-square of the function $f(t)$, a_{rms} , is defined by

$$a_{\text{rms}} = \left\{ \frac{1}{T} \int_0^T f^2(t) dt \right\}^{\frac{1}{2}} \quad (18)$$

Statistical properties of a_1, a_2, \dots, a_n , described later in this section can all be scaled relative to \bar{a} . Since it is the a_{rms} that can be related directly to the Fourier transform of $f(t)$, it is useful to derive a simple relationship between the \bar{a} and a_{rms} . For a sine wave, for example, given by

$$f(t) = A_0 \sin \omega t \quad (19)$$

$\bar{a} = A_0$ and $a_{\text{rms}} = A_0/\sqrt{2}$. For a narrow band process, that can be approximated by

$$f(t) \approx B(t) \sin \omega_0 t \quad (20)$$

we next show that

$$a_{\text{rms}} \approx \frac{\bar{a}}{\sqrt{2}} \quad (21)$$

still holds. To show that (21) is indeed correct we approximate $f(t)$ in Figure II.6 by

$$f(t) \approx a_k \sin \omega_0 t; \quad t_k \leq t \leq t_{k+1} \quad (22)$$

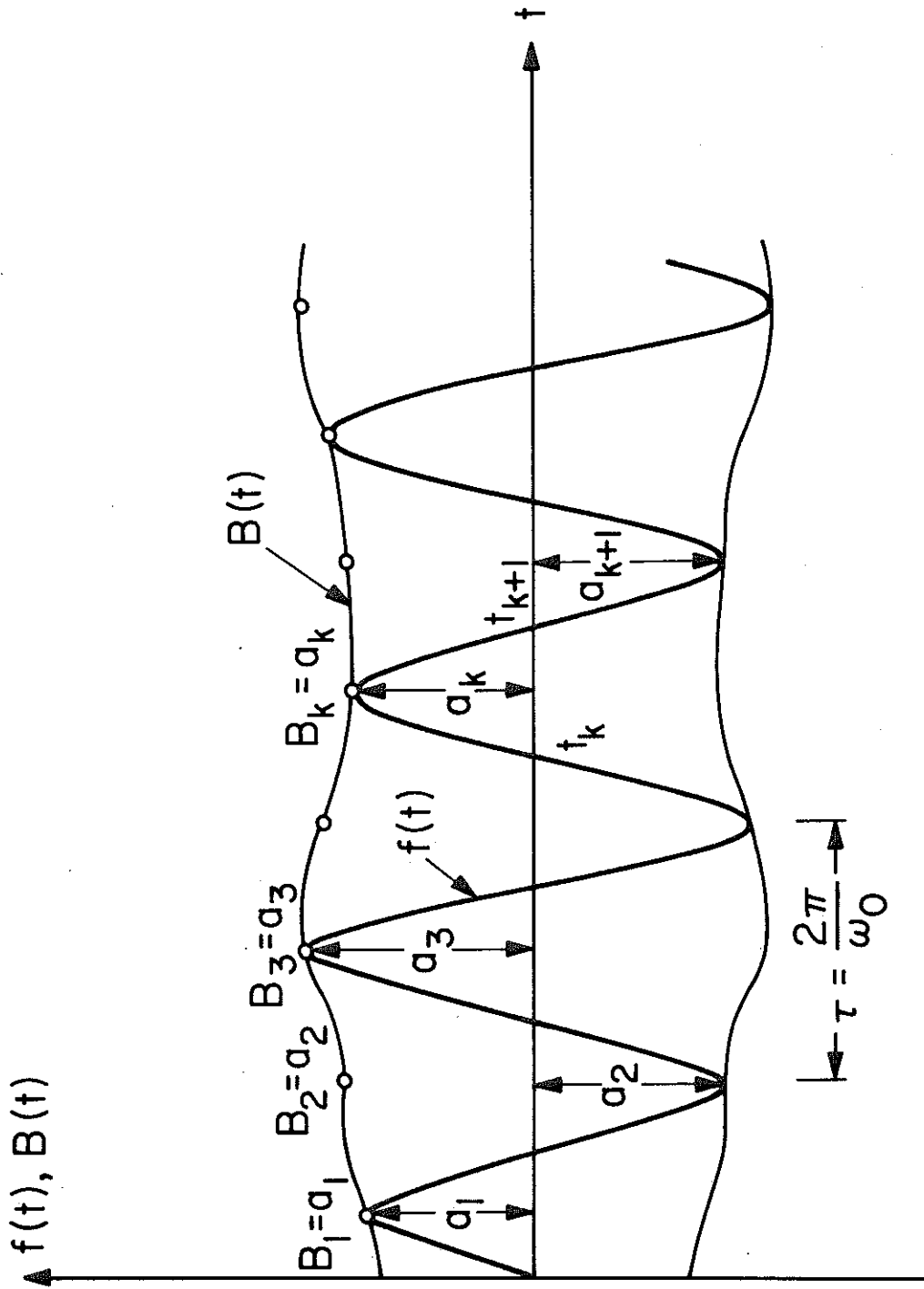


Figure II. 6 Time history of an amplitude modulated narrow band process $f(t)$ whose envelope is $B(t)$.

for $k=1, 2, \dots, n$. The root-mean-square of this approximate $f(t)$ then becomes

$$a_{\text{rms}} \approx \left\{ \frac{1}{T} \sum_{i=1}^N a_i^2 \int_0^{T/2} \sin^2 \frac{2\pi t}{T} dt \right\}^{\frac{1}{2}} = \left\{ \frac{1}{T} \frac{T}{4} \sum_{i=1}^N a_i^2 \right\}^{\frac{1}{2}} \quad (23)$$

Recalling (17) we have

$$a_{\text{rms}} \approx \frac{\bar{a}}{\sqrt{2}} \quad (24)$$

An alternate approach to the derivation of the result analogous to (21) is as follows. Again we start by assuming that (20) holds. Then the transform of the envelope $B(t)$ is $B(\omega, \omega_0)$, as shown in Figure II.7a.

Noting that

$$B(\omega, \omega_0) \equiv X(\omega, \omega_0) + iY(\omega, \omega_0) \quad (25)$$

$$F(\omega, \omega_0) \equiv Z(\omega, \omega_0) + iW(\omega, \omega_0) \quad (26)$$

and that the Fourier transform of $\sin \omega_0 t$ is $i\pi [\delta(\omega + \omega_0) - \delta(\omega - \omega_0)]$, where δ designates the delta-function, the transform of $f(t) = B(t) \sin \omega_0 t$ becomes

$$F(\omega, \omega_0) = \frac{i}{2} [B(\omega + \omega_0, \omega_0) - B(\omega - \omega_0, \omega_0)] \quad (27)$$

The real and imaginary parts of $F(\omega, \omega_0)$ are plotted in Figure II.7b. Next, observing that \bar{a} is now \bar{B} and using Parseval's theorem

$$\int_{-\infty}^{\infty} g(t) h(t) dt = \frac{1}{2\pi} \int_{-\infty}^{\infty} G(\omega) H(-\omega) d\omega \quad (28)$$

We have

$$a_{\text{rms}} = \left\{ \frac{1}{T} \frac{1}{2\pi} \int_{-\infty}^{\infty} |F(\omega)|^2 d\omega \right\}^{\frac{1}{2}} \quad (29)$$

and

$$\bar{a} = \left\{ \frac{1}{T} \frac{1}{2\pi} \int_{-\infty}^{\infty} |B(\omega, \omega_0)|^2 d\omega \right\}^{\frac{1}{2}} \quad (30)$$

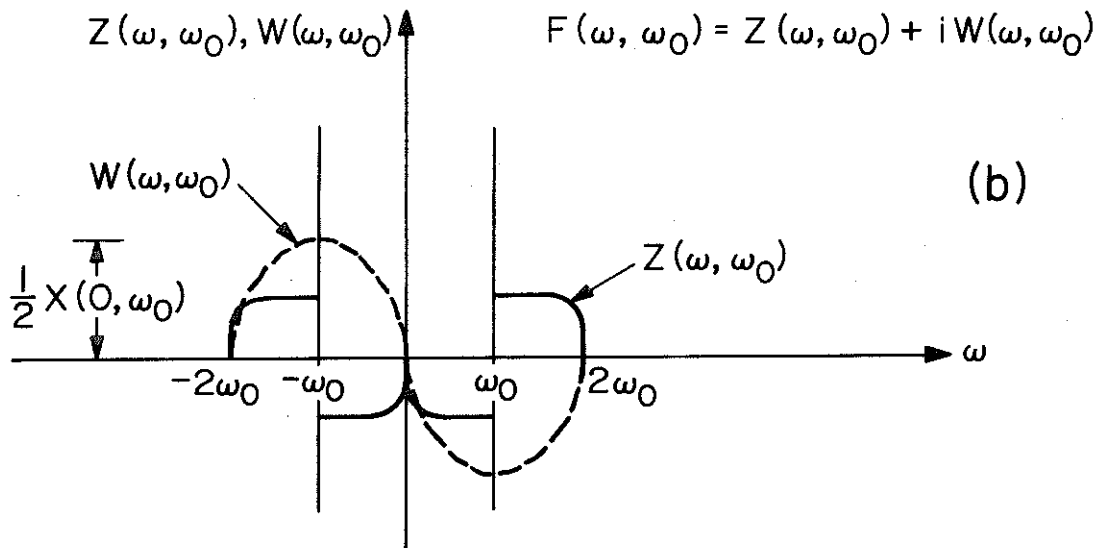
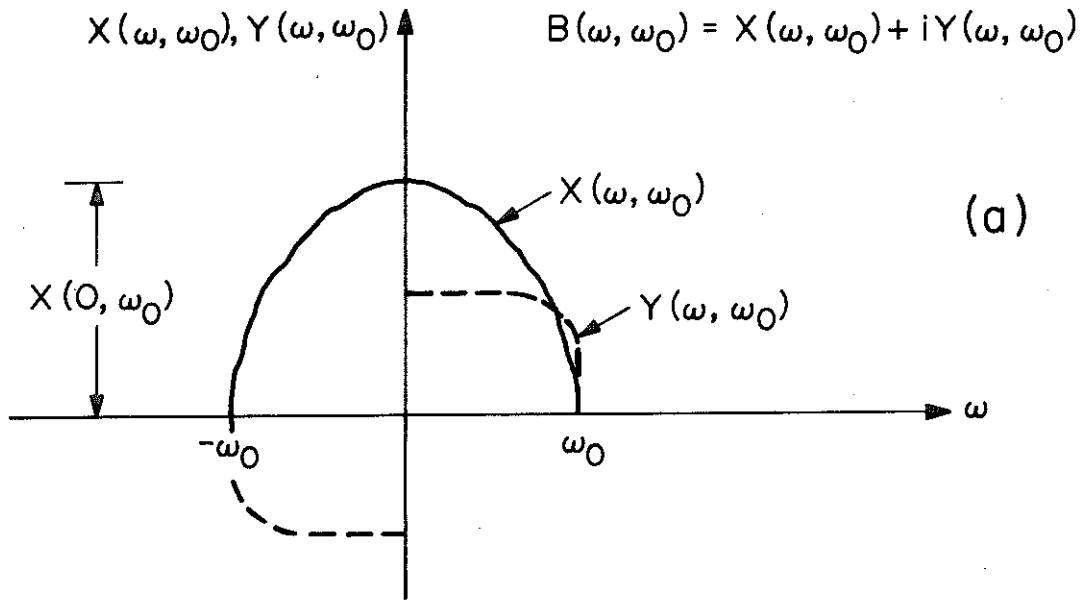


Figure II. 7

From Figure II.7 it then follows that

$$\int_{-\infty}^{\infty} |F(\omega, \omega_0)|^2 d\omega = \frac{1}{2} \int_{-\infty}^{\infty} |B(\omega, \omega_0)|^2 d\omega \quad (31)$$

and finally from (29), (30) and (31), we get (24). Using (24), \bar{a} can be calculated from a_{rms} which in turn may be computed from $F(\omega, \omega_0)$ using Parseval's theorem (28).

The Expected Value of the Maximum Wave Amplitude, $E(a_{\text{max}})$

The probability distribution of a_{max} will be derived here by assuming that the sampling of the peak amplitudes is at random. Strictly, this assumption does not hold, since the sample consists of N consecutive peaks bounded by a slowly fluctuating amplitude, and there must be some correlation between the consecutive peaks especially when the power spectrum of $f(t)$ is narrow. However, as pointed out by Longuet-Higgins⁽¹⁴⁾, fluctuations of the envelope function may act as a "randomizing" process leading to a better agreement between the observed and theoretical distributions.

Following Longuet-Higgins⁽¹⁴⁾, we begin by considering the probability that any of the a 's in the sample should be less than r

$$P\{a \leq r\} = \int_0^r \frac{2r}{a^2} e^{-\frac{r^2}{a^2}} dr = 1 - e^{-\frac{r^2}{a^2}} \quad (32)$$

It is noted here that we are considering the case of $\epsilon = 0$ corresponding to the Rayleigh distribution of peak amplitudes, with $\bar{a} = \sqrt{2}a_{\text{rms}} = \sqrt{2}m_0^{1/2}$. The probability that every a in the sample of N will be less than r becomes (assuming independence)

$$P\{a_i \leq r | i = 1, 2, \dots, N\} = \left(1 - e^{-\frac{r^2}{a^2}}\right)^N, \quad (33)$$

and the probability that at least one a shall exceed r is

$$P\{a_i \geq r | i=1, 2, \dots, N\} = 1 - \left(1 - e^{-\frac{r^2}{\bar{a}^2}}\right)^N \quad (34)$$

Using (33) and (34) the probability that a shall lie between r and $r+dr$ becomes

$$P\{r \leq a_i \leq r+dr\} = P\{a_i \geq r | i=1, 2, \dots, N\} - P\{a_i \geq r+dr | i=1, 2, \dots, N\} \quad (35)$$

and

$$P\{r \leq a_i \leq r+dr\} = -d\left[1 - \left(1 - e^{-\frac{r^2}{\bar{a}^2}}\right)^N\right]. \quad (36)$$

From (36) we have that the probability distribution of a_{\max} is

$$p(r) = N \left(1 - e^{-\frac{r^2}{\bar{a}^2}}\right)^{N-1} \frac{2r}{\bar{a}^2} e^{-\frac{r^2}{\bar{a}^2}} \quad (37)$$

The expected value of a_{\max} , $E(a_{\max})$ then becomes

$$E(a_{\max}) = \int_0^{\infty} r d\left[1 - \left(1 - e^{-\frac{r^2}{\bar{a}^2}}\right)^N\right] \quad (38)$$

and can be shown to be equal to ⁽¹⁴⁾

$$\frac{E(a_{\max})}{\bar{a}} = \frac{\sqrt{\pi}}{2} \left[\frac{N}{1!} - \frac{N(N-1)}{2!\sqrt{2}} + \frac{N(N-1)(N-2)}{3!\sqrt{3}} - \dots + (-1)^{N+1} \frac{1}{\sqrt{N}} \right] \quad (39)$$

$E(a_{\max})/\bar{a}$ is plotted in Figure II. 8 and tabulated in Table I for N between 1 and 20. For values of N larger than about 20, (39) becomes difficult to calculate because the binomial coefficients become too large for routine computations. It is of interest to consider an asymptotic expression for $E(a_{\max})/\bar{a}$ valid for large values of N . It can be shown ⁽¹⁴⁾ that this expression becomes

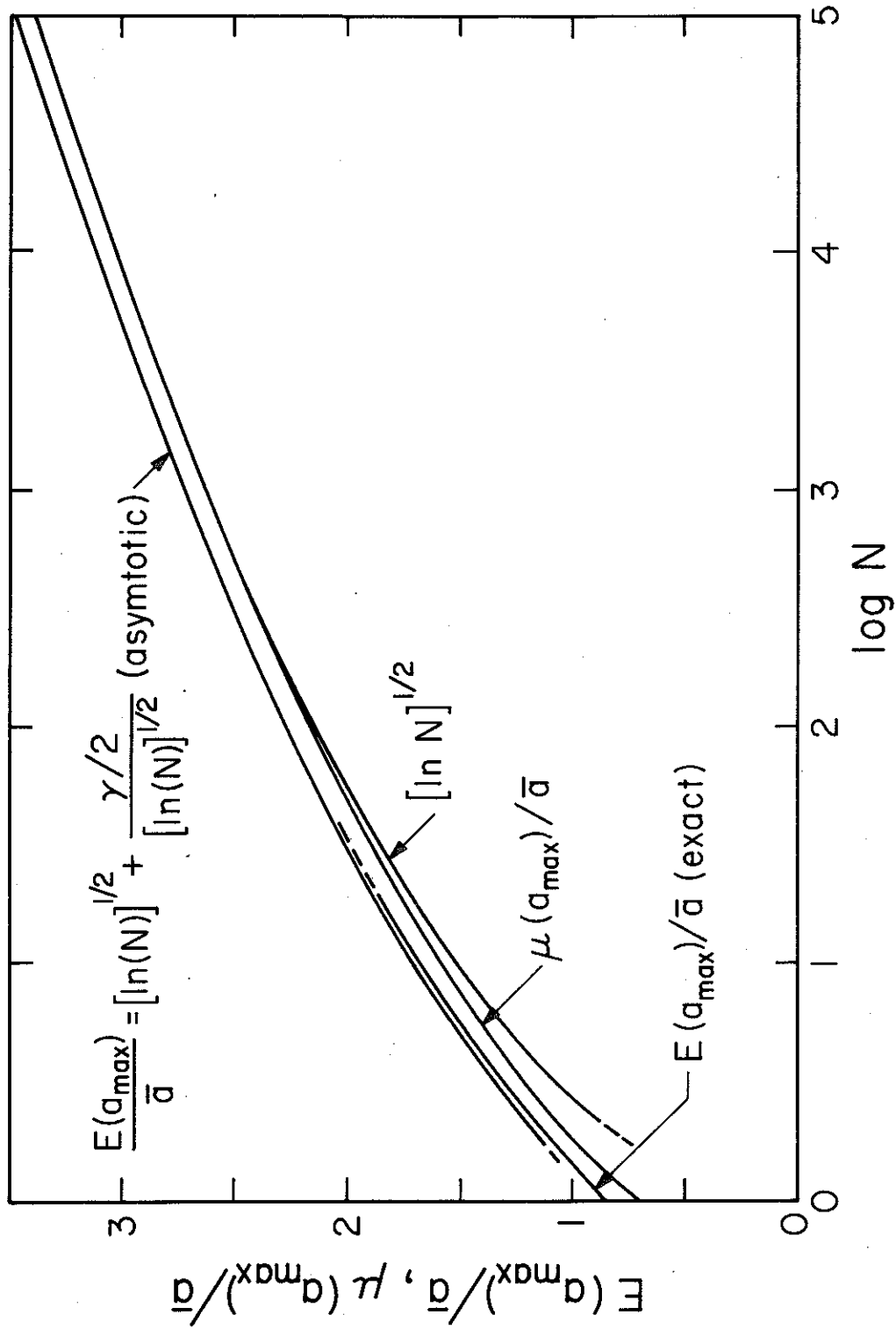


Figure II. 8 Graphs of the expected peak value $E(a_{\max})$ and the most probable value $\mu(a_{\max})$ as a function of the number of peaks for $\epsilon = 0$. Both amplitudes have been scaled by the rms value of the peak amplitudes, \bar{a} .

TABLE I

<u>N</u>	<u>E(a_{max})/\bar{a}</u>	<u>$\mu(a_{\max})/\bar{a}$</u>	<u>$[\ln N]^{\frac{1}{2}}$</u>
1	0.886	0.707	0.0
2	1.146	1.030	0.833
3	1.290	1.188	1.081
4	1.389	1.291	1.177
5	1.462	1.366	1.269
6	1.520	1.426	1.339
7	1.568	1.475	1.395
8	1.609	1.516	1.442
9	1.645	1.552	1.482
10	1.676	1.583	1.517
11	1.704	1.611	1.549
12	1.728	1.636	1.576
13	1.751	1.659	1.602
14	1.772	1.680	1.625
15	1.792	1.699	1.646
16	1.810	1.717	1.665
17	1.829	1.734	1.683
18	1.845	1.749	1.700
19	1.853	1.764	1.716
20	1.869	1.778	1.731

$$\frac{E(a_{\max})}{\bar{a}} \approx (\ln N)^{\frac{1}{2}} + \frac{1}{2} \gamma (\ln N)^{-\frac{1}{2}} \quad (40)$$

where γ is Euler's constant equal to 0.5772. This approximation is plotted in Figure II.8 and agrees well with the exact value of $E(a_{\max})/\bar{a}$. The difference between (40) and (39) is of the order of $(\ln N)^{\frac{3}{2}}$ and apparently does not affect the approximate result (40) even for small values of N (Figure II.8). For nonzero values of ϵ (40) becomes⁽¹²⁾

$$\frac{E(a_{\max})}{\bar{a}} \approx \left[\ln(1-\epsilon^2)^{\frac{1}{2}} N \right]^{\frac{1}{2}} + \frac{1}{2} \gamma \left[\ln(1-\epsilon^2)^{\frac{1}{2}} N \right]^{-\frac{1}{2}} \quad (41)$$

As $\epsilon \rightarrow 0$ (41) reduces to (40). Figure II.9 and Table II give the values of $E(a_{\max})/\bar{a}$ for $\epsilon=0, 0.2, 0.4, 0.6$ and 0.8 derived from (41). From Figure II.9, we observe that the value of $E(a_{\max})/\bar{a}$ does not vary appreciably with either N or ϵ . The most critical factor then in the determination of $E(a_{\max})$ is the value of \bar{a} . Damping in the system has two effects; it changes the r.m.s. of the response, which is related to the total energy of the oscillator and, it affects the value of ϵ , which is related to the distribution of this energy among the different frequencies.

When $\epsilon \rightarrow 1$, $(1-\epsilon^2)N$ is not large compared to 1 and the above approximation, (41) ceases to be valid. The limiting form corresponding to $\epsilon=1$, i.e., when $p(\eta)$ is normal, was considered by Fisher and Tippett⁽¹⁵⁾.

We get

$$\frac{E(a_{\max})}{\bar{a}} \approx 2^{-\frac{1}{2}} \left(m + \frac{m}{2} \right) \quad (42)$$

where m is the mode of the distribution of a_{\max} given by $(2\pi)^{\frac{1}{2}} m e^{-\frac{1}{2}m^2} = N$. Table II gives the exact values of $E(a_{\max})/\bar{a}$ calculated by Tippett⁽¹⁶⁾ for

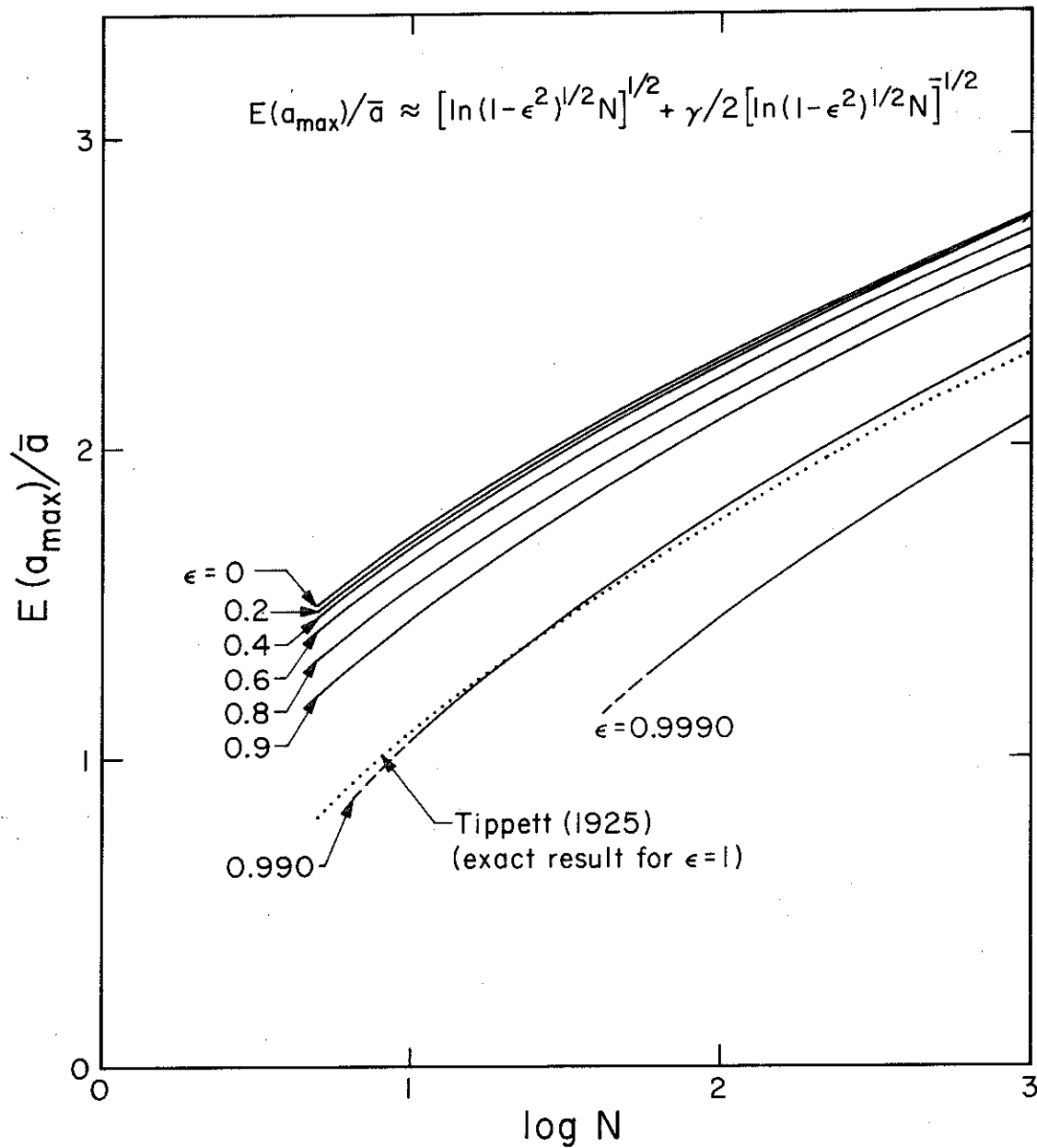


Figure II. 9 Asymptotic approximation for the expected peak value $E(a_{\max})$ when $(1-\epsilon^2)^{1/2} N$ is large.

$\epsilon=1$. However, for values of N between 10 and 1000, most frequently encountered in spectral analysis, $\epsilon=0.990$ and the approximate expression (41) give results that are within 3 percent of the exact (Tippett's) calculations (see the last two columns in Table II and, Figure II.9 for $\epsilon=0.990$).

The Most Probable Wave Amplitude, $\mu(a_{\max})$

The most probable value of a_{\max} , of course, corresponds to the peak of the probability distribution $p(r)$ (see equation (37)). Writing $r^2/\bar{a}^2 \equiv \theta$, (37) becomes

$$N(1 - e^{-\theta})^{N-1} \frac{1}{\bar{a}} \theta^{\frac{1}{2}} e^{-\theta}$$

and the most probable value of θ is then given by the solution of

$$\frac{d}{d\theta} \left[(1 - e^{-\theta})^{N-1} \theta^{\frac{1}{2}} e^{-\theta} \right] = 0 \quad (43)$$

The exact most probable value of a_{\max} , $\mu(a_{\max})$, calculated from (43) is tabulated in Table I for $N \leq 20$ and plotted in Figure II.8 for $N \leq 10^5$. Performing the differentiation in (43) and taking the natural logarithm of the result gives⁽¹⁴⁾

$$\theta = \ln N - \ln \left[1 - \frac{1}{2\theta} (1 - e^{-\theta}) \right] \quad (44)$$

When N is large we have

$$\theta = \ln N + O(\ln N)^{-1} \quad (45)$$

and thus

$$\frac{\mu(a_{\max})}{\bar{a}} = \theta^{\frac{1}{2}} \approx [\ln N]^{\frac{1}{2}} \quad (46)$$

Approximation (46) is given in Table I and is plotted in Figure II.8. The results show that for $N \geq 100$ (46) becomes an excellent approximation to $\frac{1}{\theta^2}$.

TABLE II

<u>N</u>	<u>E(a_{max}) / ā</u>						
	$\epsilon^+ = 0$	$\epsilon^* = 0.2$	$\epsilon^* = 0.4$	$\epsilon^* = 0.6$	$\epsilon^* = 0.8$	$\epsilon^* = 0.990$	$\epsilon^+ = 1.0$
5	1.496	1.490	1.468	1.423	1.323	-	0.822
10	1.708	1.701	1.682	1.642	1.554	1.079	1.088
20	1.898	1.892	1.875	1.838	1.759	1.301	1.321
50	2.124	2.119	2.103	2.071	2.001	1.604	1.587
100	2.280	2.276	2.261	2.231	2.166	1.804	1.773
200	2.427	2.423	2.409	2.381	2.320	1.985	1.942
500	2.609	2.605	2.592	2.565	2.509	2.203	2.147
1000	2.738	2.734	2.722	2.697	2.643	2.354	2.292

* Approximation (41)

+ Exact (Tippett, 1925)

The Upper Bound Confidence Level For a_{\max}

Here we consider the probability of a_{\max} exceeding a given level, with the objective of calculating an estimate of the upper bound of a_{\max} that depends on N and the preselected probability that a_{\max} will not exceed it. We choose to call this curve "the upper bound confidence level" and designate it by $a_{\text{MAX}, C}$, where C specifies the confidence level selected.

It was shown above that the probability distribution of a_{\max} is

$$p(r) = \frac{d}{dr} \left[\left(1 - e^{-\frac{r^2}{\bar{a}^2}} \right)^N \right] \quad (37)$$

The probability that a_{\max} will exceed a given level r is then given by

$$p(r) = \int_r^{\infty} d \left[\left(1 - e^{-\frac{r^2}{\bar{a}^2}} \right)^N \right] = 1 - \left(1 - e^{-\frac{r^2}{\bar{a}^2}} \right)^N \quad (47)$$

By defining r_0 by the equations

$$\frac{r_0^2}{\bar{a}_0^2} \equiv \theta_0 = \ln N; \quad e^{-\frac{(r_0^2/\bar{a}^2)}{N}} = \frac{1}{N} \quad (48)$$

Longuet-Higgins⁽¹⁴⁾ has shown that

$$\frac{d}{dr} \left(1 - \frac{e^{-(r^2 - r_0^2)/\bar{a}^2}}{N} \right)^N \approx \frac{d}{dr} e^{-e^{-(r^2 - r_0^2)/\bar{a}^2}} \quad (49)$$

The approximate probability that a will be less than r is therefore

$$e^{-Ne^{-(r^2/\bar{a}^2)}} \quad (50)$$

and that it will be greater than r is

$$p_0 = 1 - e^{-Ne^{-(r^2/\bar{a}^2)}} \quad (51)$$

The exact and approximate results, (47) and (51), are compared in Figure II. 10 and it is seen that for $N \geq 10$ (51) becomes an excellent approximation to (47).

The upper bound confidence level $a_{MAX, C}$ becomes the solution of the following equation

$$1 - \left(1 - e^{-\left(a_{MAX, C}^2 / \bar{a}^2\right)}\right)^N = 1 - C \quad (52)$$

or, using the approximate probability p_0 , given by (51), it becomes

$$1 - e^{-N e^{-\left(a_{MAX, C}^2 / \bar{a}^2\right)}} = 1 - C \quad (53)$$

Solving for $a_{MAX, C} / \bar{a}$ in (52) we obtain

$$\frac{a_{MAX, C}}{\bar{a}} = \left[-\ln\left(1 - C^{\frac{1}{N}}\right) \right]^{\frac{1}{2}} \quad (54)$$

and from (53)

$$\frac{a_{MAX, C}}{\bar{a}} = \left[\ln\left(\frac{-N}{\ln C}\right) \right]^{\frac{1}{2}} \quad (55)$$

Both (54) and (55) are tabulated in Table III for three typical values of C and for values of N up to 10,000. The agreement between the exact and approximate results is excellent. Ten different $a_{MAX, C} / \bar{a}$ curves for C ranging from 0.90 to 0.99 are compared with $E(a_{max}) / \bar{a}$ curve for $\epsilon=0$ in Figure II. 11.

Applications to Response Spectrum Analysis

The response $r(t)$ of an oscillator subjected to an input ground motion $-\ddot{z}(t)$ can be obtained in frequency space as the product of the transfer function of the oscillator and the Fourier transform of $\ddot{z}(t)$. It shall be assumed in what follows that the oscillator started from rest.

TABLE III

<u>N</u>	<u>$a_{MAX}, C/\bar{a}$</u> (exact)	<u>$a_{MAX}, C/\bar{a}$</u> (approximate)	<u>C</u> (confidence level)
1	2.146	2.145	0.99
10	2.627	2.627	0.99
100	3.034	3.034	0.99
1,000	3.392	3.392	0.99
10,000	3.715	3.716	0.99
1	1.731	1.723	0.95
10	2.297	2.296	0.95
100	2.752	2.752	0.95
1,000	3.143	3.143	0.95
10,000	3.490	3.490	0.95
1	1.517	1.500	0.90
10	2.135	2.134	0.90
100	2.618	2.618	0.90
1,000	3.026	3.026	0.90
10,000	3.385	3.385	0.90

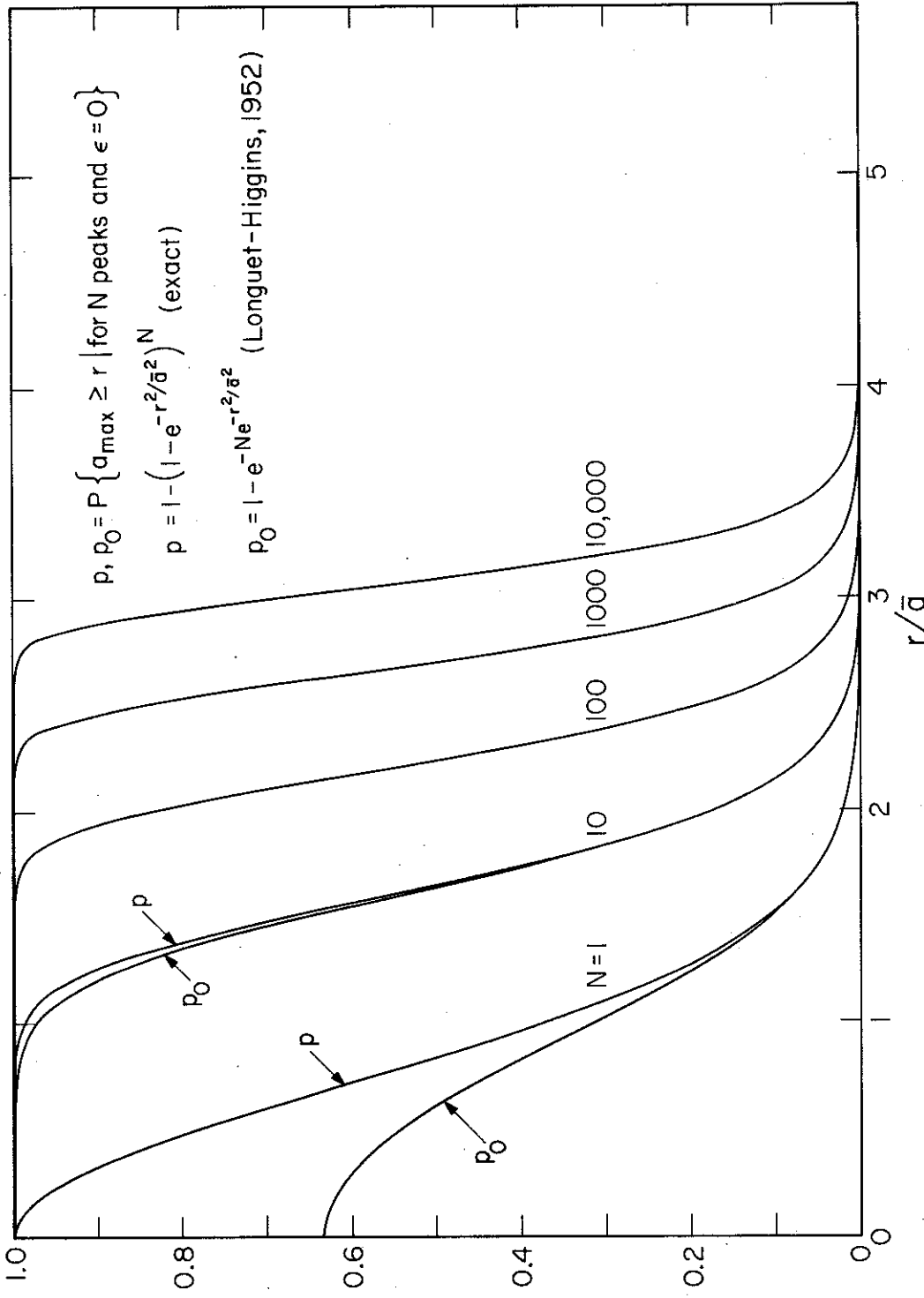


Figure II.10 Probability of a_{\max} exceeding the level r for N peaks with $\epsilon = 0$.

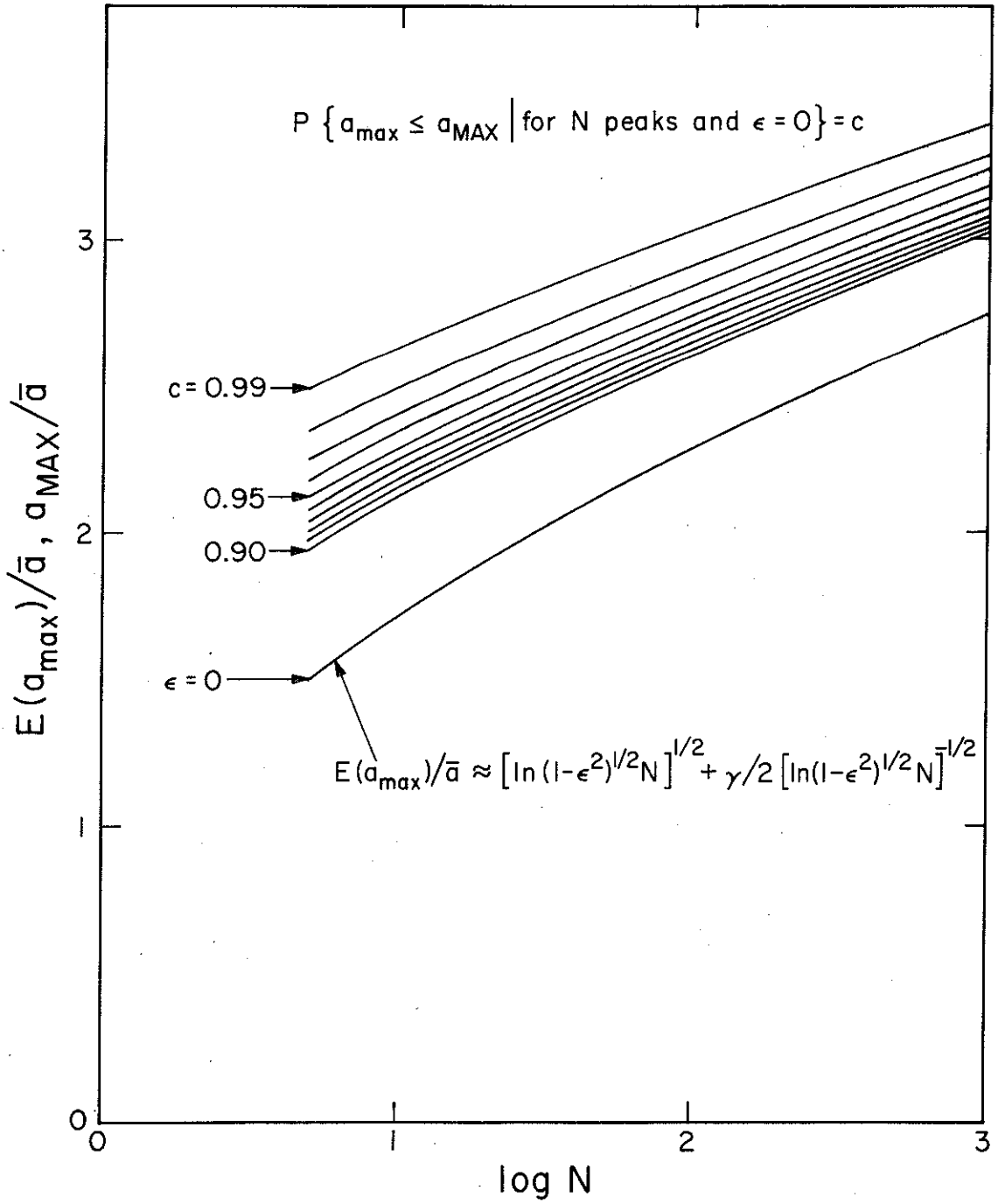


Figure II.11 Upper bounds for a_{\max} for different confidence levels plotted versus the logarithm of the number of peaks.

Hence

$$R(\omega) = H(\omega) Z(\omega)$$

where $H(\omega)$ is the transfer function of the oscillator, $Z(\omega)$ is the transform of the input function, and $R(\omega)$ is the response.

As seen from the previous section, the two parameters which influence the response of such an oscillator are ϵ , which is a measure of the distribution of energy among the various frequencies, and a_{rms} , which is a measure of the total energy of the system. The computation of a_{rms} can be done in terms of the values of $H(\omega)$ and $Z(\omega)$ as follows

$$a_{\text{rms}}^2 = \frac{1}{T} \int_0^T r^2(t) dt = \frac{1}{2\pi T} \int_{-\infty}^{\infty} |R(\omega)|^2 d\omega = \frac{1}{2\pi T} \int_{-\infty}^{\infty} |H(\omega)|^2 |Z(\omega)|^2 d\omega \quad (56)$$

$$a_{\text{rms}}^2 = \frac{1}{\pi T} \int_0^{\infty} |H(\omega)|^2 |Z(\omega)|^2 d\omega \quad (57)$$

This can be easily calculated for any given input and any desired oscillator transfer function $H(\omega)$. The corresponding values of ϵ can then be calculated by computing the zeroth, second, and fourth moments of $|R(\omega)|$.

Next an estimate of the total number of maxima, N , is required. We shall assume here that the oscillator acts as a narrow band filter and that the value of N can be taken as the ratio of the duration of the record and the fundamental period T of the oscillator. A knowledge of these parameters enables the calculation of the expected value of the maximum peak (Equation (41)), the expected value of the most probable peak (Equation (46)), and the 95 percent confidence level (Equation (55)).

Statistics on the pseudo velocity were obtained by multiplying by ω each of the three quantities statistically determined. Statistics on the velocity spectrum were generated by considering the function $(\omega R(\omega))^2$ instead of $(R(\omega))^2$ in Equation (56).

A Case Study on Three Accelerograms

The statistical approach outlined above has a large number of assumptions. The ability of the method to give an indication of the velocity and pseudo velocity spectra was checked using three different types of real accelerograms.

The first accelerogram used was the Eureka 1954 record shown in Figure I.2a. The acceleration consists of a short burst of energy about five seconds long preceded and followed by much smaller motions. Figure II.12a and 12b show the pseudo velocity and the velocity spectral curves. The lowermost curve is the damped Fourier spectrum drawn for 2 percent damping, while the statistical curves are indicated by dashed and dotted lines. The calculated true and pseudo velocity spectrum ($\xi = 0.02$) are shown by circles. The length of record analyzed was 20 seconds.

We note that the damped Fourier spectrum curve ($\xi = 0.02$) is below the pseudo velocity and velocity spectrum points (full circles) ($\xi = 0.02$). From our discussion in Part I, this is exactly what we would expect. These damped spectral curves can then be used as lower bounds for the damped velocity spectra. Statistical curves for frequencies below 2 cps show good correlations with the computed velocity and pseudo velocity spectra. However, at higher frequencies rather large divergences (5-10 percent) occur. This is caused by the nonstationary nature of the excitation. The lack of high frequency contents in the signal tends to reduce the scaling factor, \bar{a} , when averages over longer and longer time lengths are taken. However, we observe that the general trend in the statistical curves do follow the trends in the velocity and pseudo velocity spectra.

To study this point further 2 percent damping curves were calculated

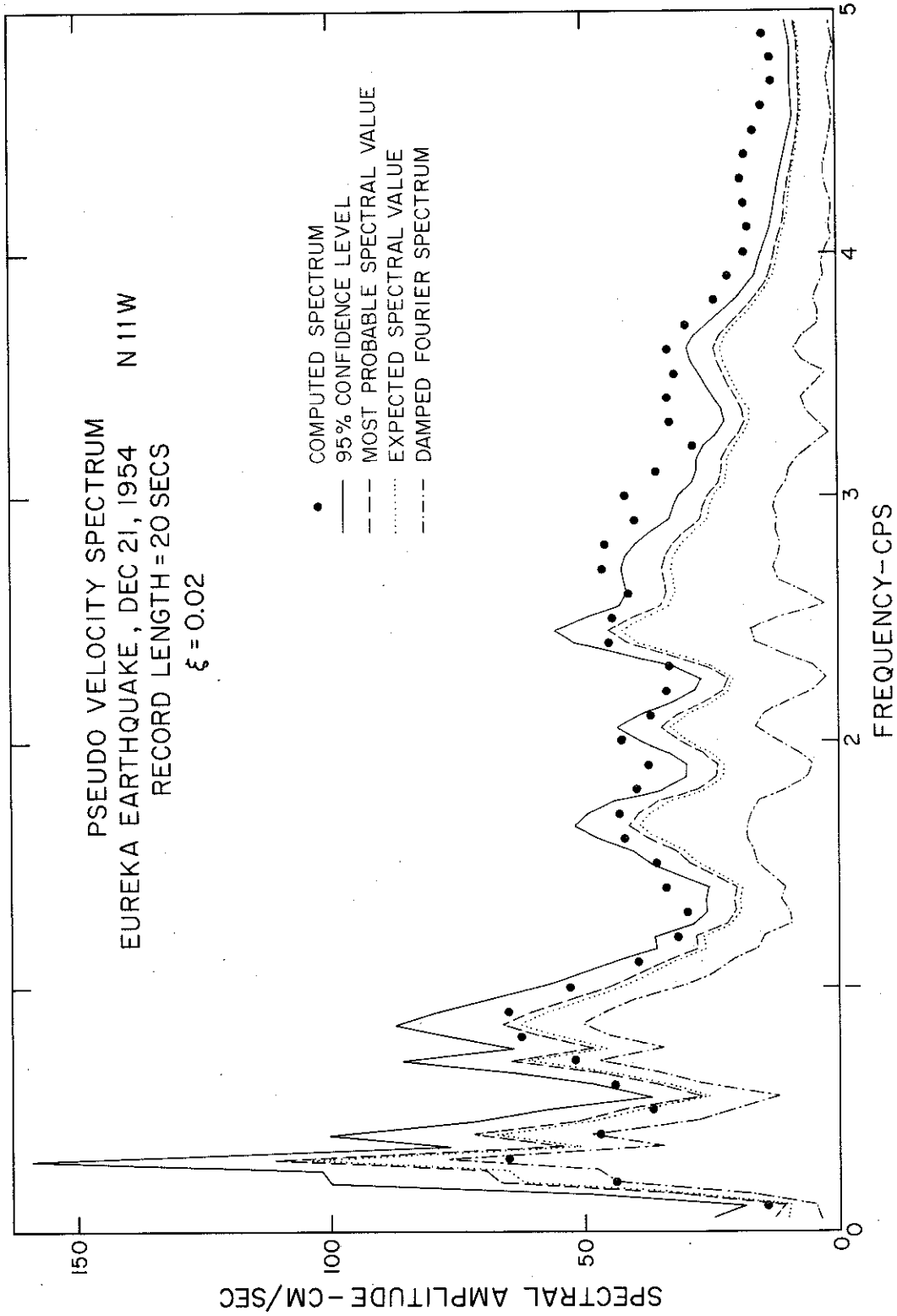


Figure II.12(a) The pseudo velocity spectrum, the damped Fourier spectrum and statistical estimates for a 20 second length of the Eureka accelerometer (Figure I.2(a)).

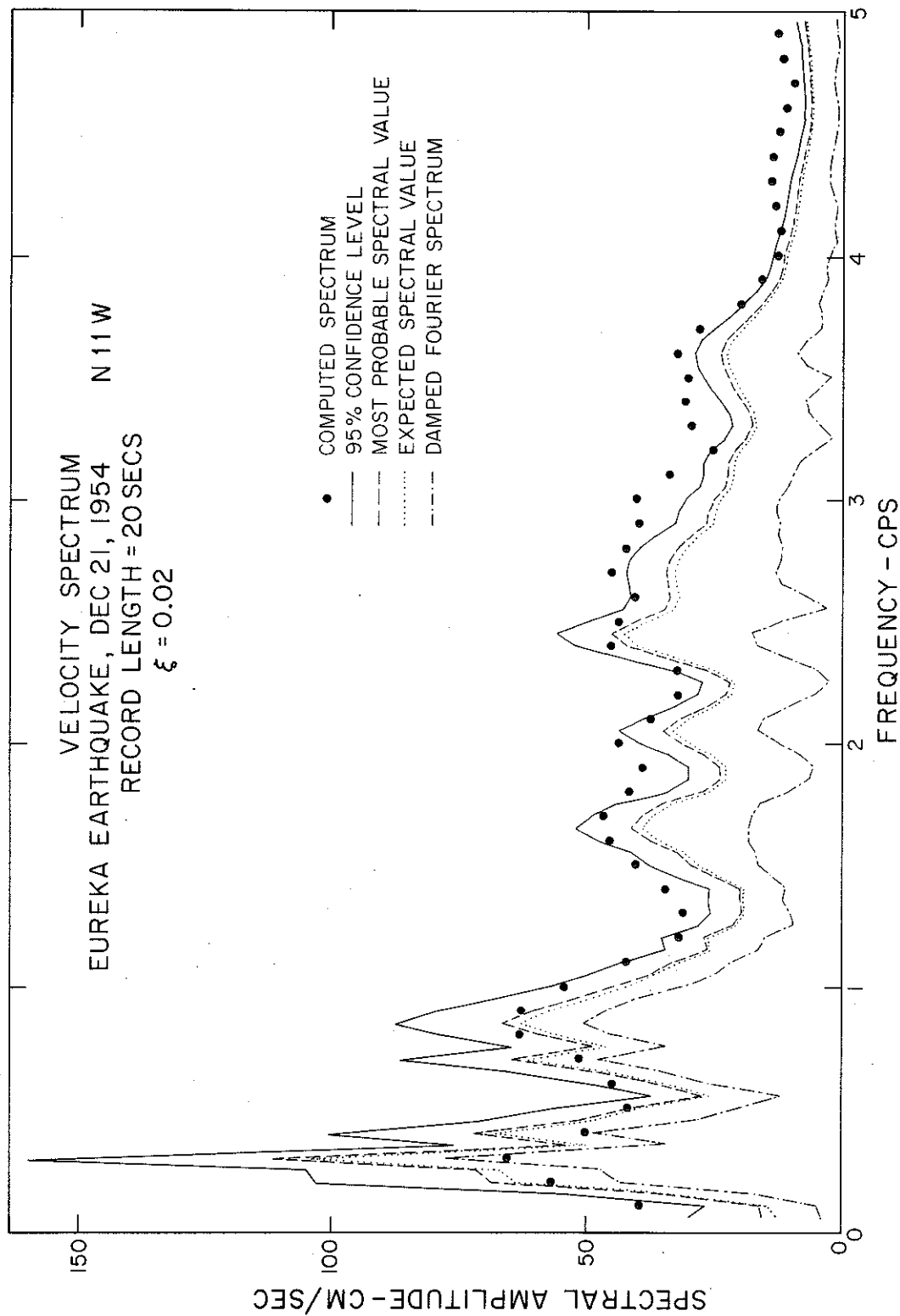


Figure II.12(b) The velocity spectrum, the damped Fourier spectrum and statistical estimates for a 20 second length of the Eureka accelerometer (Figure I.2(a)).

for the first 10 seconds of record (Figure II.13a and b). We observe an improved correlation between the statistical bounds and the calculated spectral values up to about 4 cps.

The next accelerogram tested was the El Centro event of 1940. The curves corresponding to a 30 second length of this accelerogram (Figure I.2b) show a good correlation all the way to 5 cps (Figure II.14a and b). The near stationary response of a lightly damped oscillator to this acceleration history makes the statistical estimates excellent indications of the true spectral values.

The third accelerogram tested was the Kern County accelerogram (Figure I.2c). This accelerogram is representative of a large number of real accelerograms in that it starts off with the high frequency arrivals (S and P waves) and carries on with the various surface wave modes. As we go along the accelerogram, the frequency content changes, there being less and less higher frequency components in the surface wave arrivals. Thirty-five seconds of record were analyzed, and the 2 percent damped spectra were obtained as shown in Figure II.15a and b. The figures show that up to about 1.8 cps the spectral points (full circles) are pretty much straddled by the damped Fourier spectrum curve and the 95 percent confidence level curve. At higher frequencies again a noticeable fall off in the statistical values occurs. The maximum difference between the statistically expected maxima and the actual spectral values is about 10 percent.

The above three accelerograms have been chosen as representatives of a large number of real accelerograms obtained during strong ground shaking. The results indicate that statistical studies can be made very fruitfully if we consider lengths of record which are stationary with respect to the frequencies of interest to us. The fact that the higher

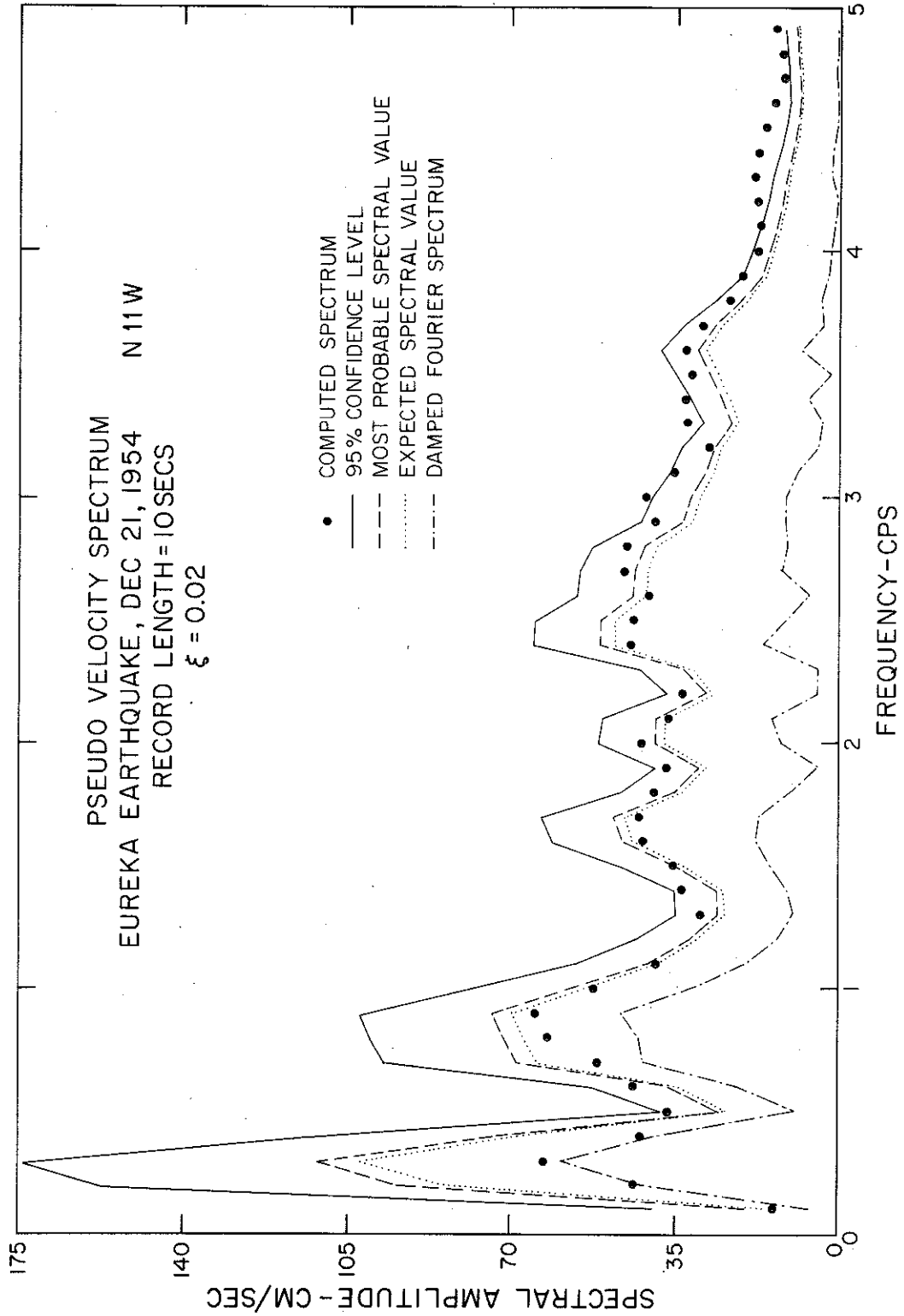


Figure II.13(a) The pseudo velocity spectrum, the damped Fourier spectrum and statistical estimates for a 10 second length of the Eureka accelerometer (Figure I.2(a)).

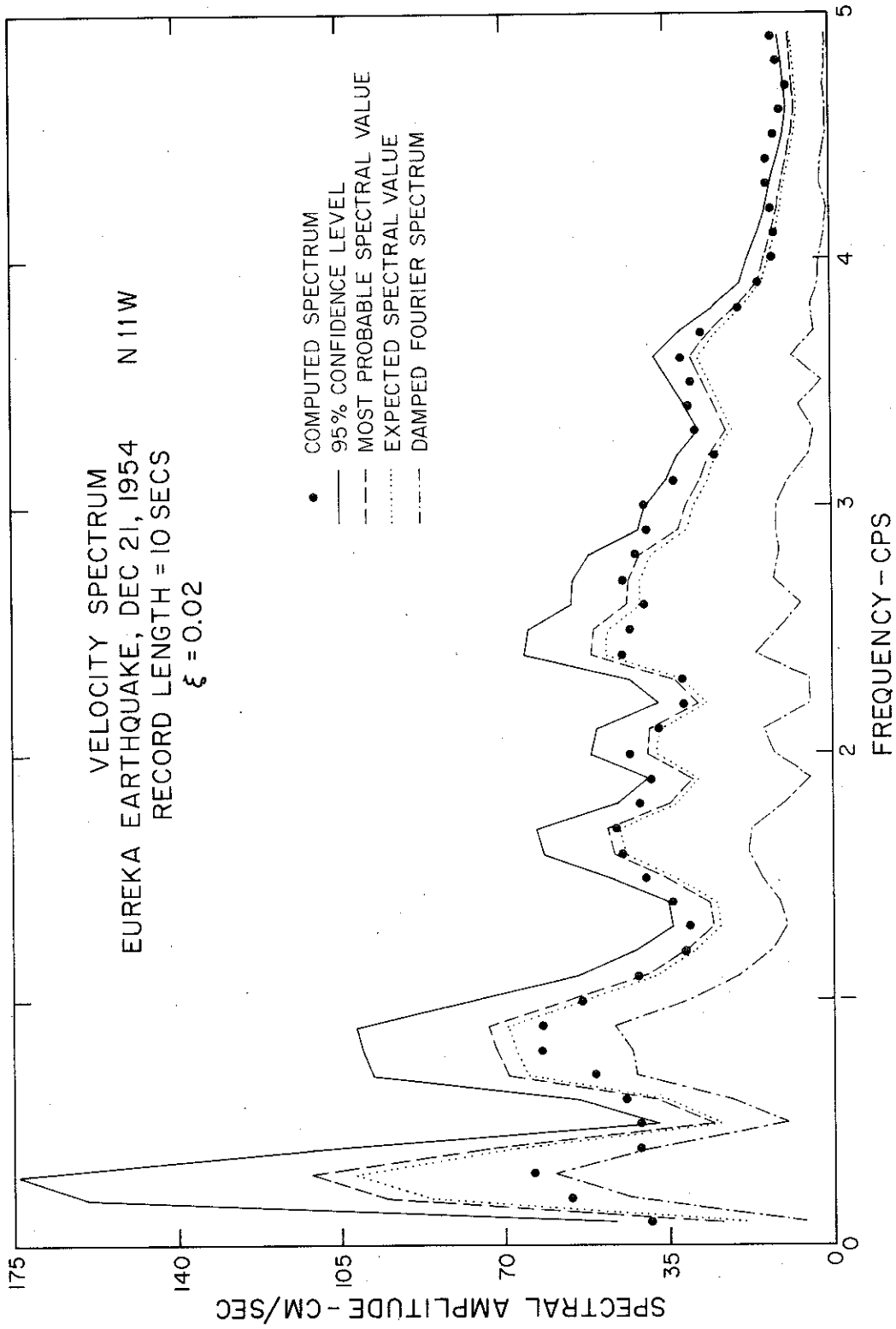


Figure II. 13(b) The velocity spectrum, the damped Fourier spectrum, and statistical estimates for a 10 second length of the Eureka accelerometer (Figure I.2(a)).

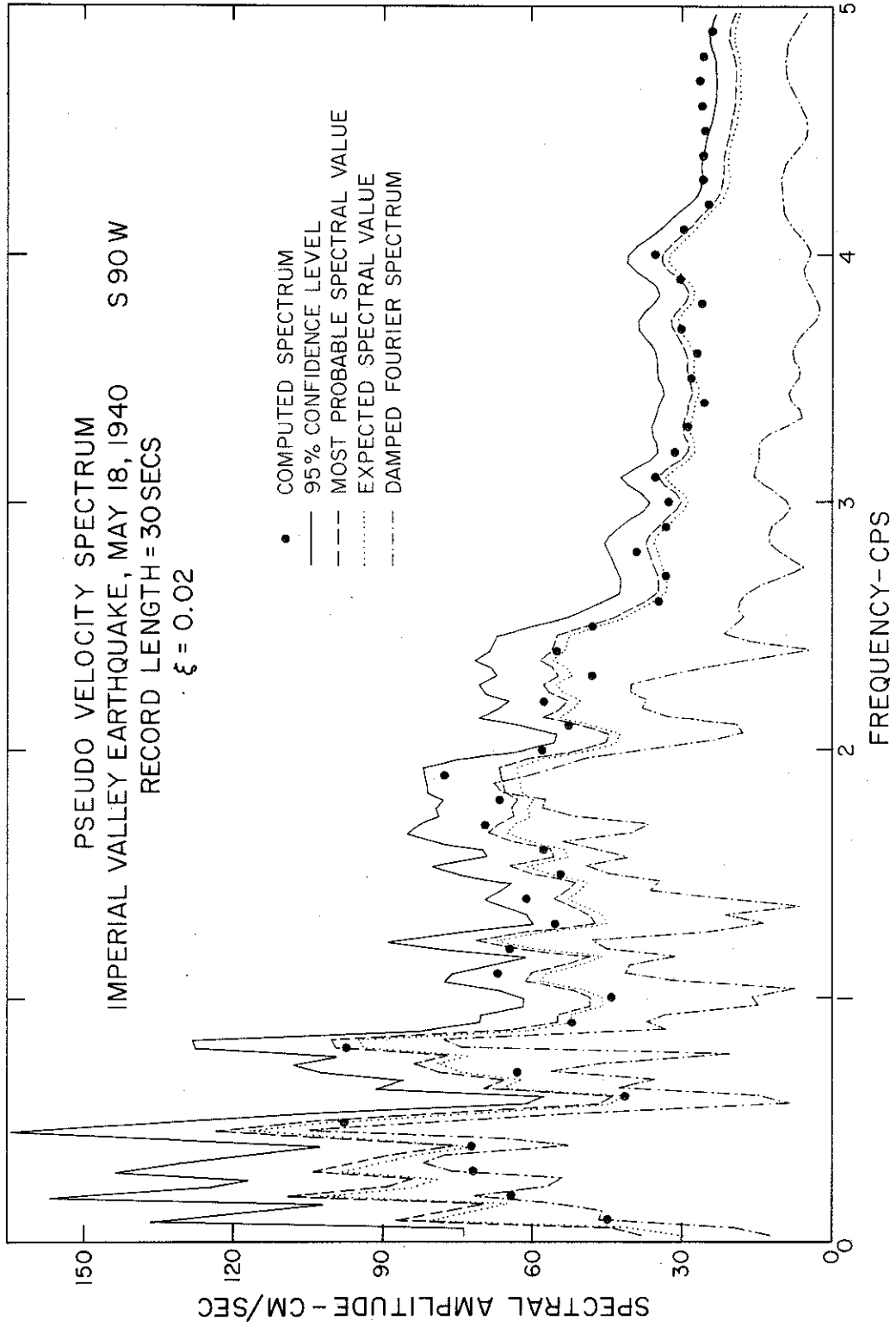


Figure II.14(a) The pseudo velocity spectrum, the damped Fourier spectrum and the statistical estimates for a 30 second length of the El Centro accelerometer (Figure I.2(b)).

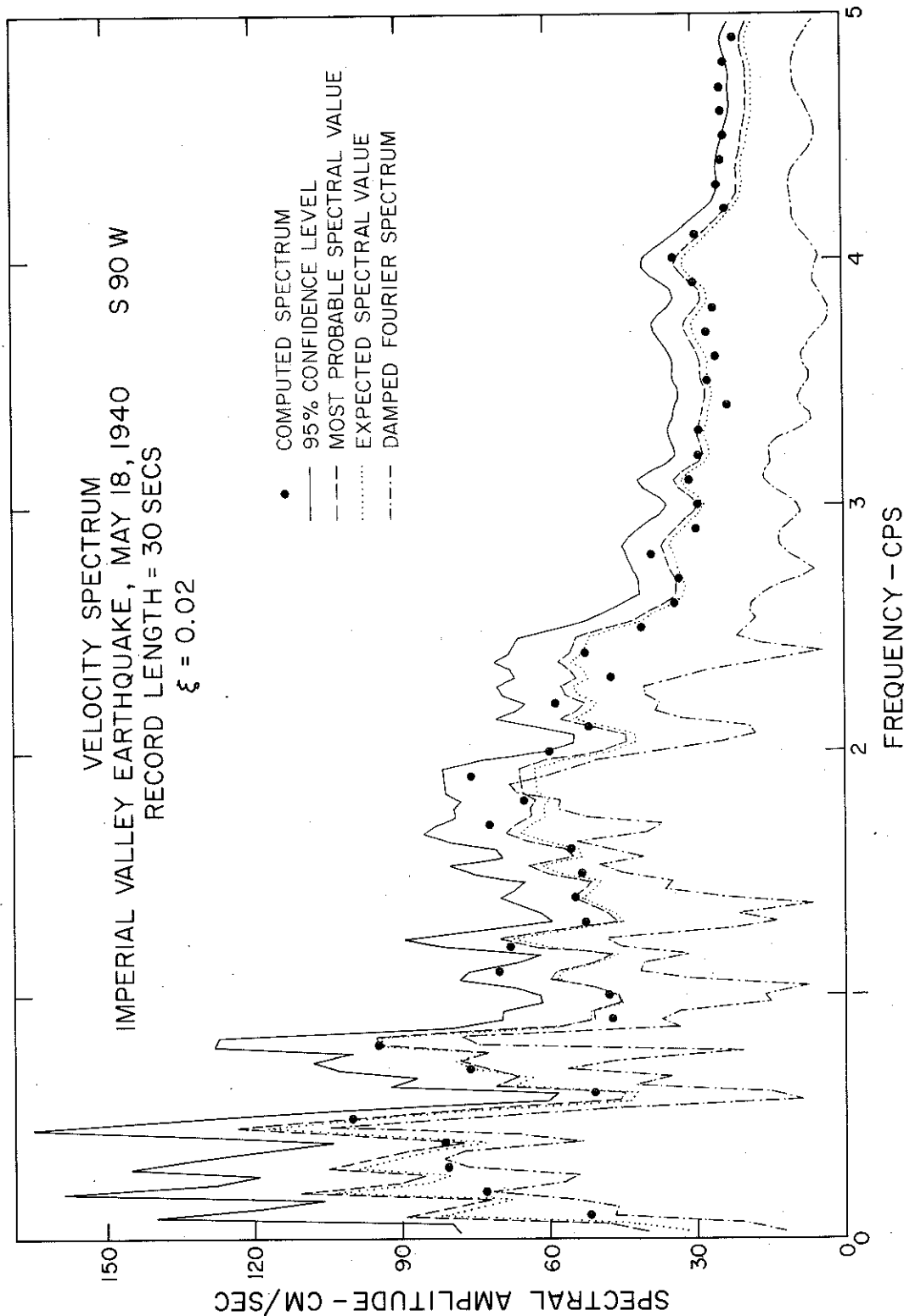


Figure II.14(b) The velocity spectrum, the damped Fourier spectrum and the statistical estimates for a 30 second length of the El Centro accelerometer (Figure I.2(b)).

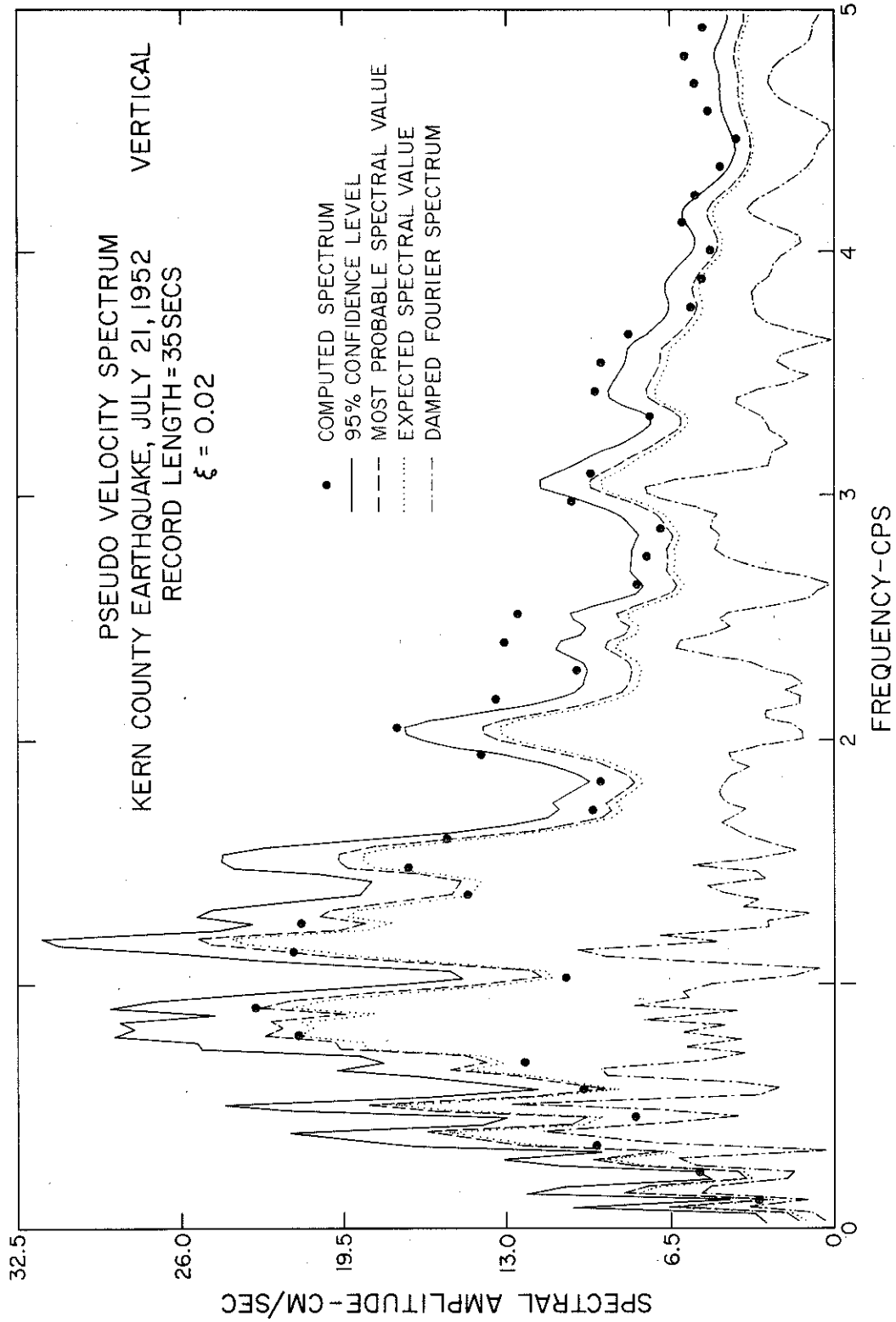


Figure II.15(a) The pseudo velocity spectrum, the damped Fourier spectrum and the statistical estimates for a 35 sec length of the Kern County accelerogram (Figure I.2(c)).

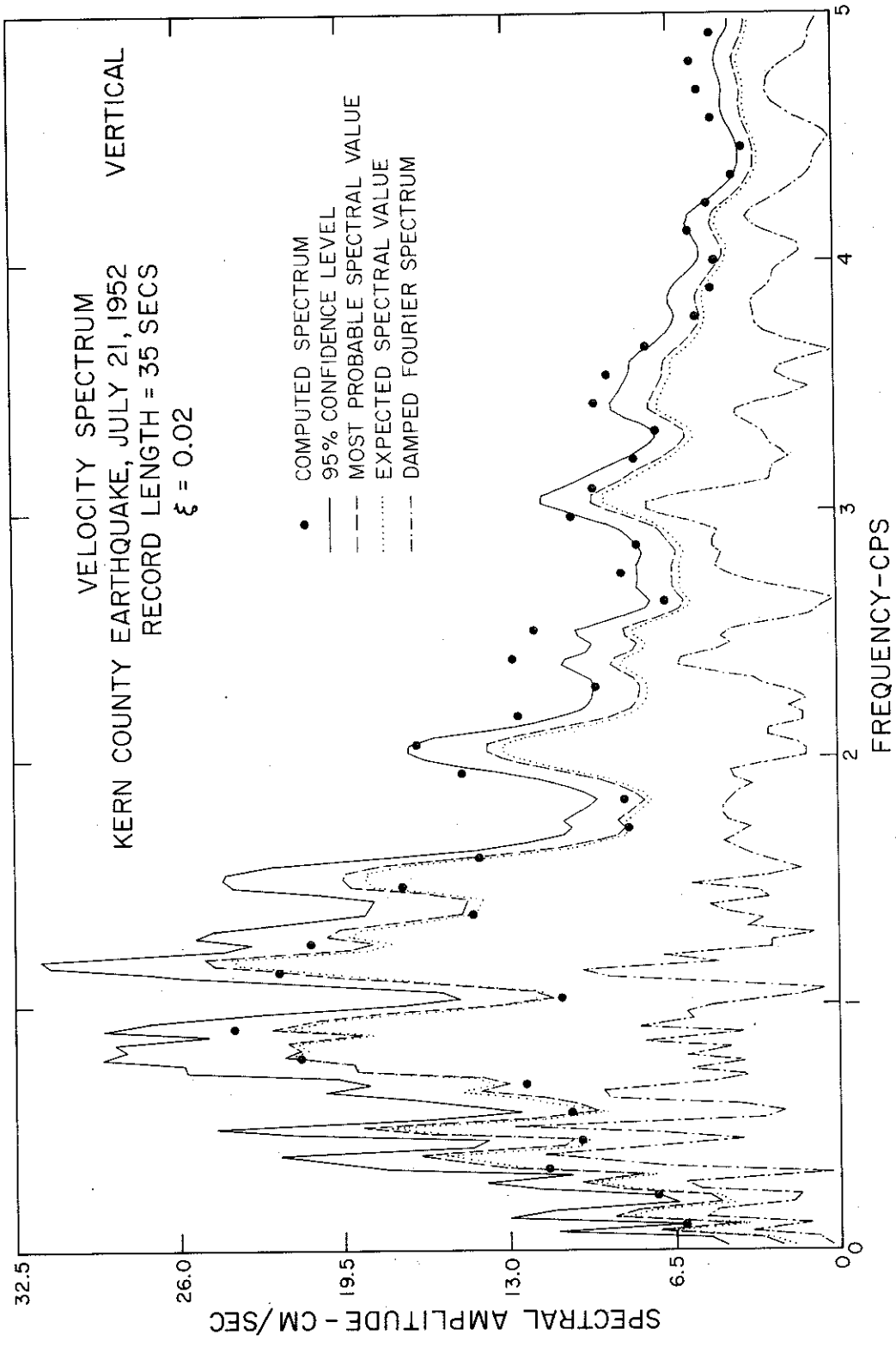


Figure II.15(b) The velocity spectrum, the damped Fourier spectrum and the statistical estimates for a 35 sec length of the Kern County accelerometer (Figure I.2(c)).

frequency components dies out earlier in the record necessitates a shorter time segment of record for statistical analysis of real accelerograms to get better estimates at higher frequencies, than would be generally required for longer periods. However, the lengths of the record analyzed should contain a sufficiently large number of cycles (at least 4-5) of the oscillator so as to make such a statistical approach meaningful.

Discussion

The chief assumption in the derivation of the results of Section II.a are (1) that the signal being analyzed is stationary in time and (2) that the frequency spectrum is a narrow band.

To check the statistical estimates, a study on white noise was performed. Two samples of white noise (referred to as white noise No. 1 and white noise No. 5) were considered. Figure II.16 shows a white noise acceleration record. The computed spectra together with the statistical estimates are shown in Figure 17. The figures show excellent agreement for frequencies beyond about 1 cps. At frequencies below 1 cps, the statistical estimates tend to be above the actual computed values. This has been principally attributed to the numerical errors in integration which arise when the transfer function $H(\omega)$ is peaked around zero frequency. These errors tend to overestimate the area expressed by Equation (57). In order to minimize this error, the Fourier transform was linearly interpolated between two consecutive frequency estimates and the area then computed. A better method would be the use of the sampling theorem to define $Z(\omega)$ continuously and then an integration of the product $Z(\omega)H(\omega)$. Also, it must be remembered that statistical estimates for values of N which are less than 2 or 3 may not be meaningful, for the analysis assumes

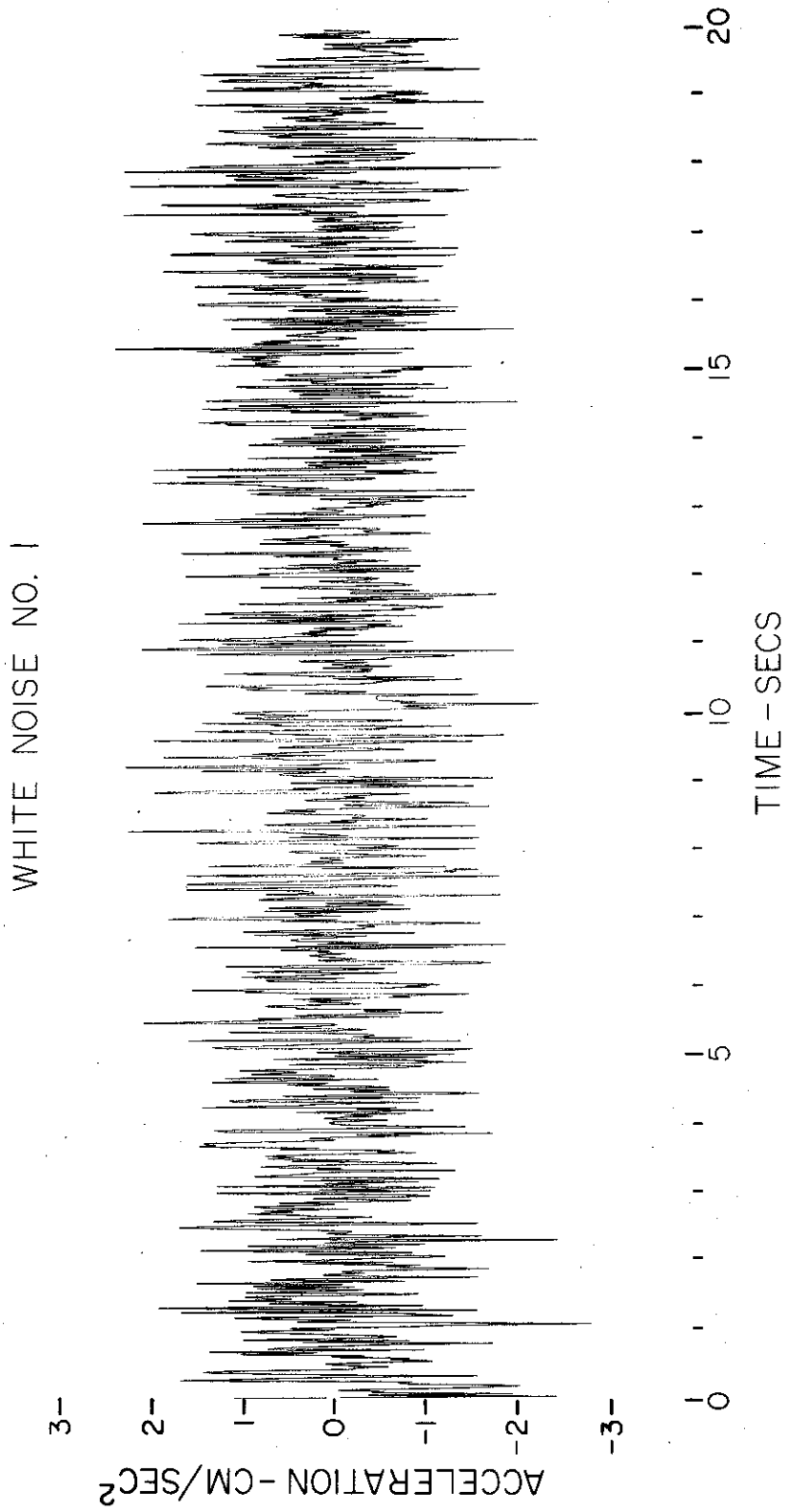


Figure II. 16 Acceleration time history of white noise No. 1.

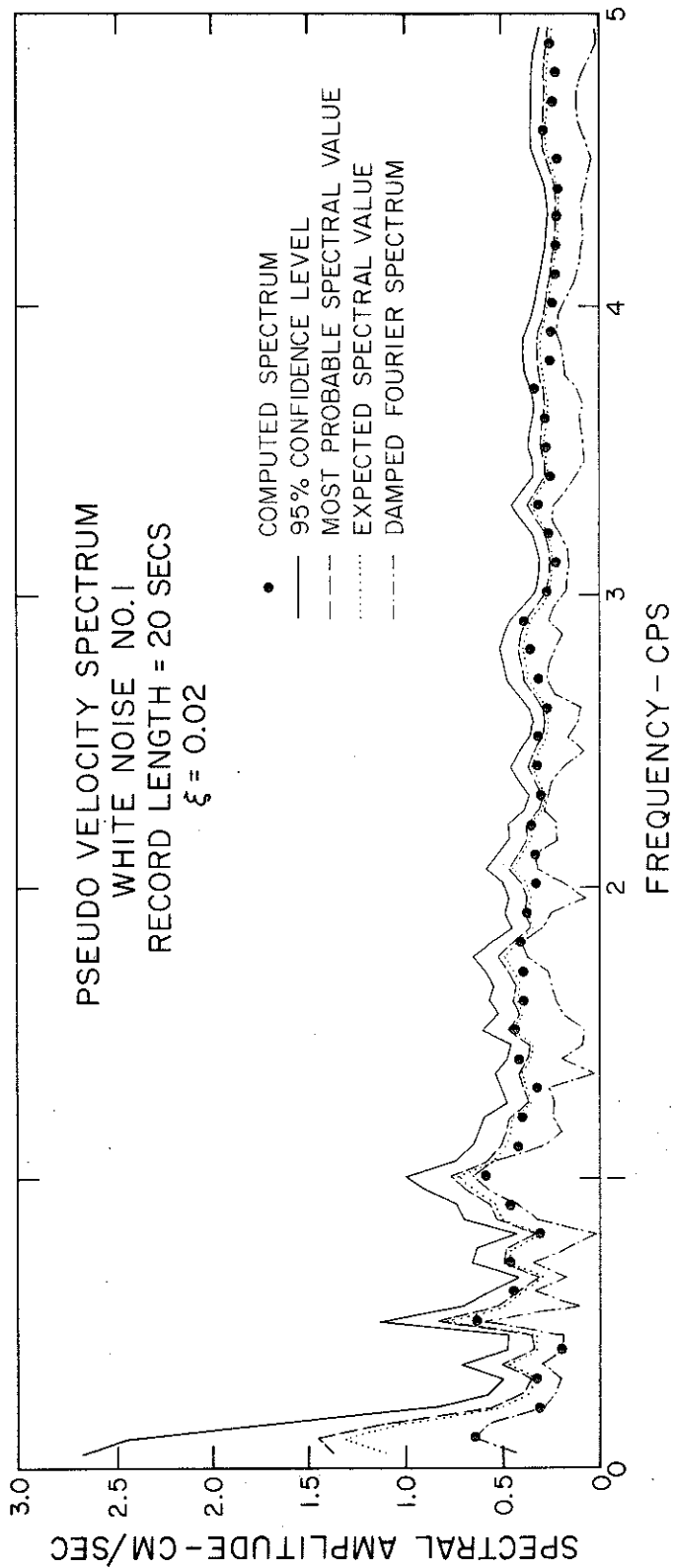


Figure II. 17(a) Pseudo velocity spectrum, damped fourier spectrum and statistical estimates for a 20 second length of white noise No. 1 of Figure II. 16.

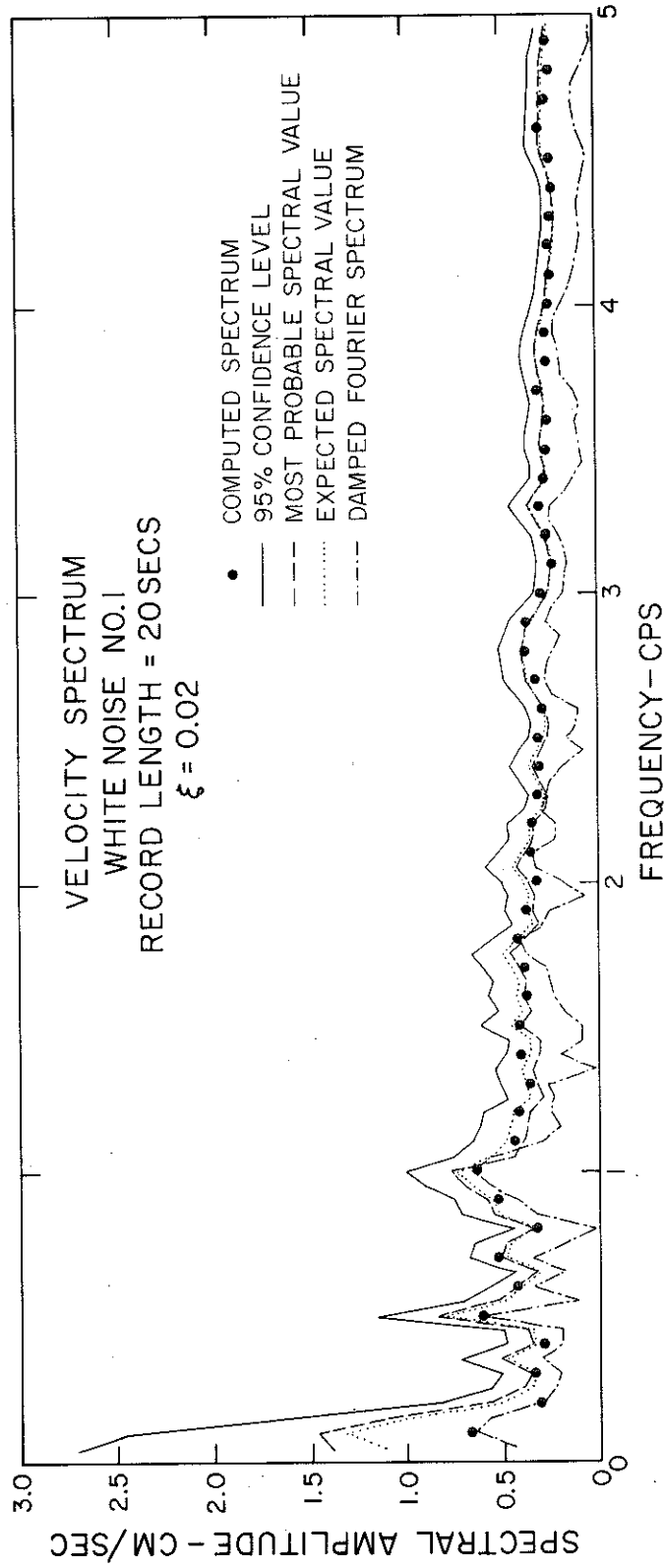


Figure II. 17(b) The velocity spectrum, the damped fourier spectrum and the statistical estimates for a 20 second length of white noise No. 1 of Figure II. 16.

that the time length of record is long enough to ensure that the sample of wave heights is sufficiently representative.

The effect of various percentages of damping has been indicated for white noise No. 5 (Figure II.18), in Figures II.19, II.20 and II.21. We observe that larger and larger amounts of damping cause the function $H(\omega)$ to be less and less peaked, hence reducing the numerical inaccuracies at the lower frequency end of the spectrum.

In addition to the overestimation of the spectral amplitudes at lower frequencies ($N \leq 4$), other errors arise in dealing with real accelerograms. Here the major problem is the lack of stationarity of the data. At any given site, the motions created by an earthquake indicate the arrivals of various phases at various times. Characteristically, the S and P waves which arrive early in the complete time history show larger proportions of higher frequency contents than the later arrivals of the longer period surface waves. A proper statistical analysis based on the assumption of stationarity would require that the time length of recording chosen not be too long, so that in this time the frequencies and amplitudes do not change significantly. This has already been illustrated through the study of two different time lengths of the Eureka earthquake record (Figures II.12 and II.13).

Furthermore, the effect of damping which leads to an exponential decay of an oscillator once the excitation has stopped would tend to underestimate the root-mean-square value of the response, in general, thus leading to underestimates of the spectral values (Figure II.22). We observe (Figure II.22) that low statistical estimates are obtained for $\xi = 0.1$ almost always lying below the pseudo velocity values computed. The figure once more illustrates the excellent correlation of trends in the

WHITE NOISE NO. 5

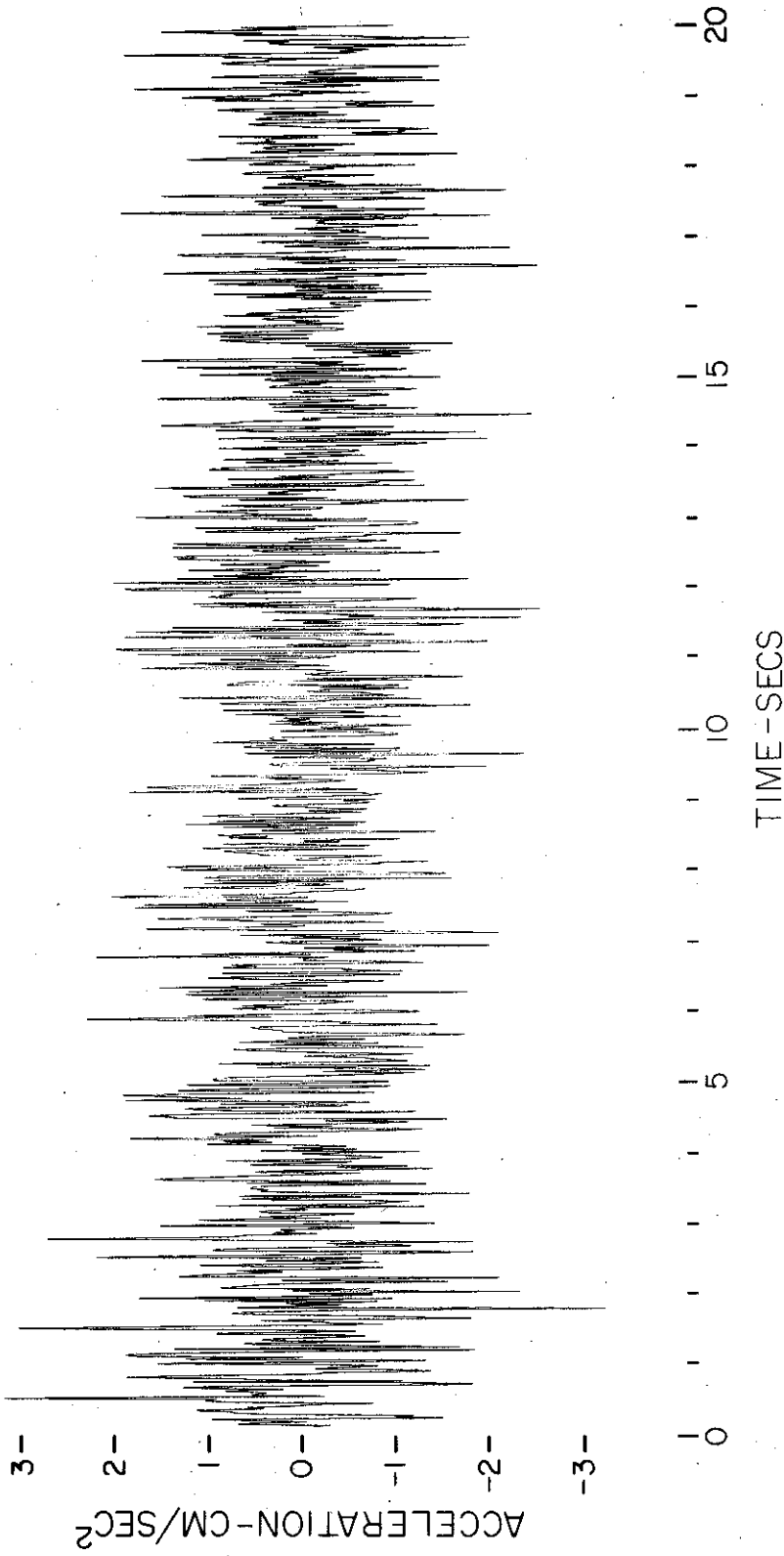


Figure II. 18 Acceleration time history of white noise No. 5.

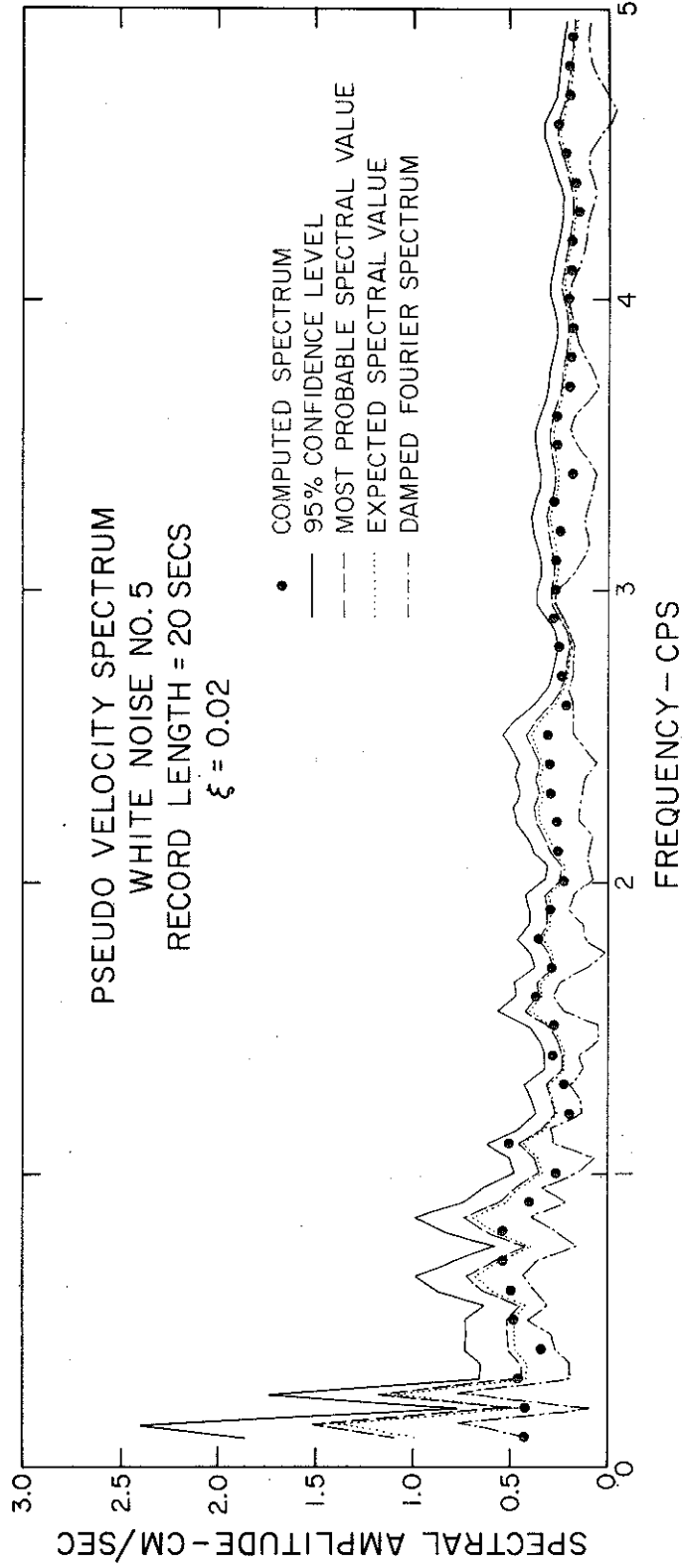


Figure II. 19 Pseudo velocity spectrum, damped fourier spectrum and statistical estimates for white noise No. 5 (Figure 18) with $\xi = 0.02$.

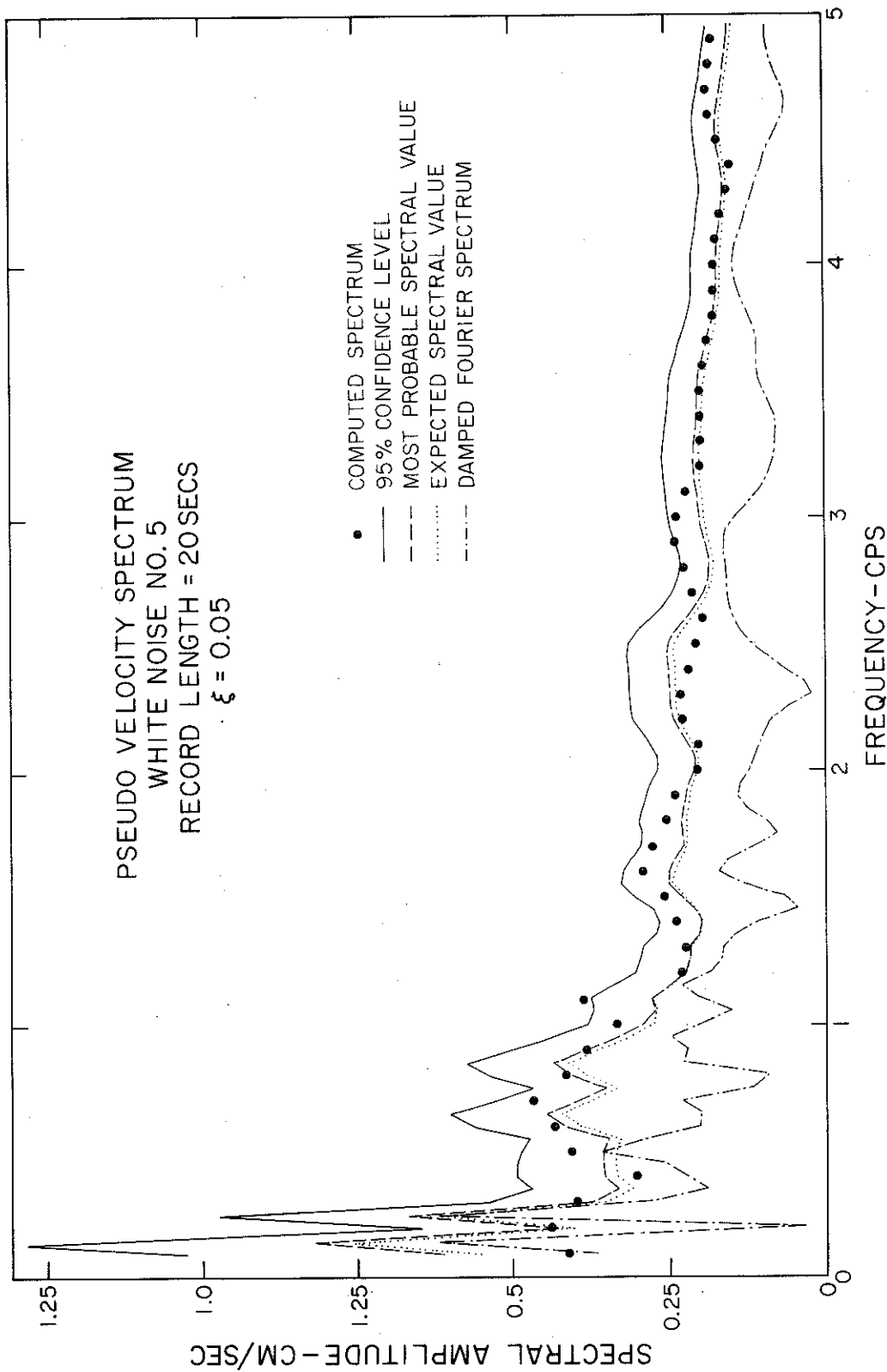


Figure II. 20 Pseudo velocity spectrum, damped fourier spectrum and statistical estimates for white noise No. 5 (Figure 18) with $\xi = 0.05$.

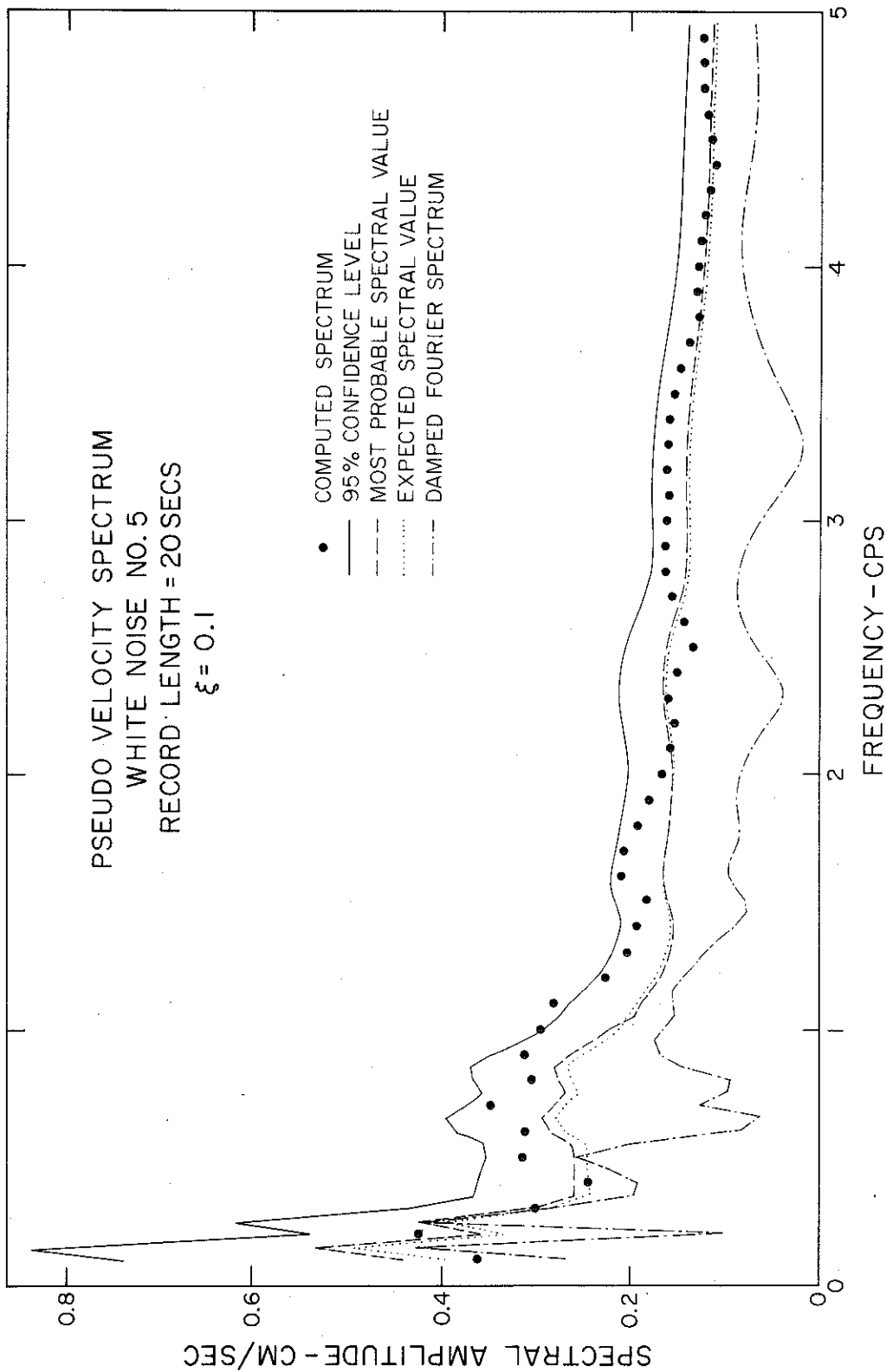


Figure II. 21 Pseudo velocity spectrum, damped fourier spectrum and statistical estimates for white noise No. 5 (Figure 18) with $\xi = 0.1$.

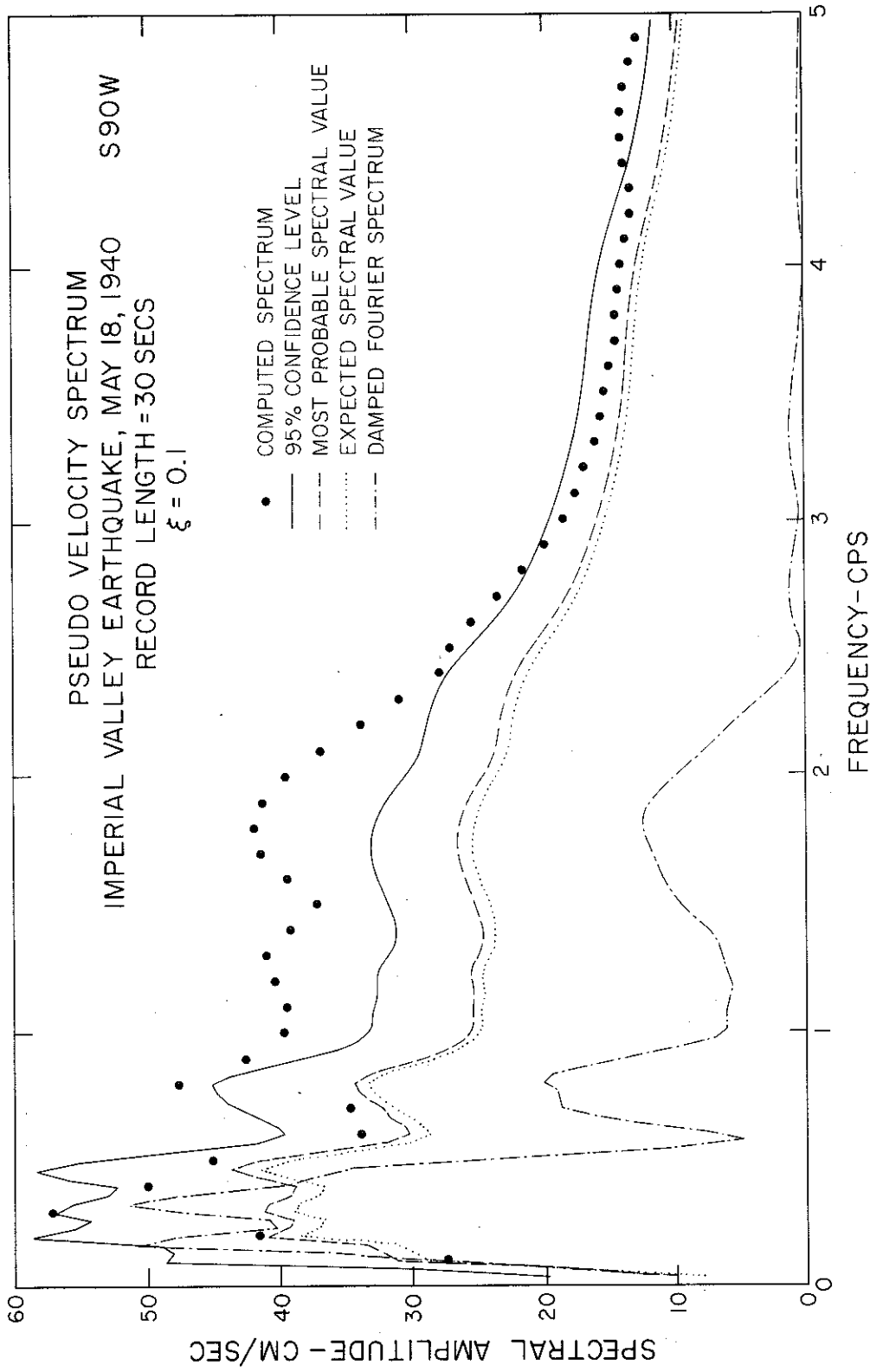


Figure II. 22 Pseudo velocity spectrum, damped fourier spectrum and statistical estimates for the El Centro accelerometer (Figure II. 2(b)) with $\xi = 0.1$.

10 percent damped Fourier amplitude spectrum and the 10 percent damped pseudo velocity curves. The damping ratio also affects ϵ . Larger damping ratios will generally lead to larger ϵ 's and broader band processes. Though the most probable level and the confidence level curves correspond to values of $\epsilon = 0$, they can be used as conservative upper bounds for $\epsilon = 0$ since these curves for $\epsilon = 0$ will cause an overestimation of the spectral estimates.

CONCLUSIONS

It has been illustrated that given the Fourier transform of the input ground motion $\ddot{Z}(t)$, statistical estimates of the maximum response of any single degree of freedom linear system can be easily determined if the assumption of stationarity is approximately satisfied. The two parameters of importance are the relative distribution of energy among the various frequencies and the r.m.s. level. These parameters depend on the nature of the input spectrum and on the damping ratio of the oscillator. Larger damping ratios cause relatively wider response energy spectra and hence lead to increased values of ϵ . Typically, for most earthquakes the values of ϵ tend to be between about 0.2 and 0.5. When $\epsilon \rightarrow 0$, we get to a pure sinusoid while with $\epsilon \rightarrow 1$, $p(\eta)$ tends to a Gaussian distribution.

Though the assumption of stationarity is far from correct in dealing with real accelerograms, it has been demonstrated that with a judicious choice of the time of the record, estimates of the damped spectra to within 10 to 15 percent of the true values can be easily obtained. The success of the statistical method is greatly due to relative insensitivity of factors such as the estimated number of waves and the spectral width ϵ . Its strong dependence on the r.m.s. level is, however, a serious limitation

in that it requires a careful choice of the time length needed to simulate stationary conditions.

Extensions of this statistical approach to amplitude modulated stationary signals will no doubt yield even better comparisons with actual velocity and pseudo velocity spectra. However, even there, the change in the frequency content with time in a non-random manner would be a serious limitation.

ACKNOWLEDGEMENTS

We are indebted to Professors G. W. Housner and P. C. Jennings for critical reading of the manuscript and many valuable suggestions.

This research was supported in part by Grants from the National Science Foundation and the Earthquake Research Affiliates Program at the California Institute of Technology.

REFERENCES

- (1) Udawadia, F. E. and M. D. Trifunac, "Ambient Vibration Tests of Full Scale Structures," Proceedings of the 5th World Conference on Earthquake Engineering, Rome, 1973.
- (2) Trifunac, M. D., "Tectonic Stress and the Source Mechanism of the Imperial Valley, California, Earthquake of 1940," Bull. Seism. Soc. Am., 62, No. 5, 1283-1302, 1972.
- (3) Housner, G. W., "Behaviour of Structures during Earthquakes," A. S. C. E., Eng. Mech. Div., EM4, 109-129, 1959.
- (4) Trifunac, M. D., Udawadia, F. E. and A. G. Brady, "High Frequency Errors and Instrument Corrections of Strong Motion Accelerograms," Earthquake Engineering Research Laboratory, EERL 71-05, California Institute of Technology.
- (5) Papoulis, A., "The Fourier Integral," McGraw-Hill, Electronic Sciences Series, 1962.
- (6) Holloway, J. L., "Smoothing and Filtering of Time Series and Space Fields," Advances in Geophysics, 4, 351-389, 1958.
- (7) Robinson, E. A. and S. Treitel, "Principles of Digital Filtering," Geophysics, Vol. XXIX, No. 3, 395-404, June, 1964.
- (8) Tukey, J. W., "An Introduction to the Calculations of Numerical Spectrum Analysis," in Spectral Analysis of Time Series, edited by Bernard Harris, John Wiley, New York, 25-46, 1967.
- (9) Housner, G. W., Jennings, P. C., and N. C. Tsai, "Simulated Earthquake Motions," Earthquake Engineering Research Laboratory, California Institute of Technology, 1968.
- (10) Trifunac, M. D., "Response Envelope Spectrum and Interpretation of Strong Earthquake Ground Motion," Earthquake Engineering Research Laboratory, EERL 70-06, California Institute of Technology, 1970.
- (11) Udawadia, F. E., "Investigation of Earthquake and Microtremor Ground Motions," Earthquake Engineering Research Laboratory, EERL 72-02, California Institute of Technology, 1972.
- (12) Cartwright, D. E. and M. S. Longuet-Higgins, "The Statistical Distribution of Maxima of a Random Function," Proc. Roy. Soc. London, Ser. A, 212-232, 1956.
- (13) Rice, S. O., "Mathematical Analysis of Random Noise," in Selected Papers on Noise and Stochastic Processes, edited by Nelson Wax, Dover, New York, 1954.

- (14) Longuet-Higgins, M. S. , "On the Statistical Distribution of the Heights of Sea Waves," Journal of Marine Research, No. 3, 245-266, 1952.
- (15) Fisher, R. A. and L. H. C. Tippett, "Limiting Forms of the Frequency Distribution of the Largest or Smallest Member of a Sample," Proc. Camb. Phil. Soc., 24, 180-190, 1928.
- (16) Tippett, L. H. C. , "On the Extreme Individuals and the Range of Samples taken from a Normal Population," Biometrika, 17, 364-387, 1925.